Title: Critical residues and contacts within domain IV of Autographa californica multiple nucleopolyhedrovirus GP64 contribute to its refolding during membrane fusion

Qianlong Yu[1,2], Lisha Bai[1], Ning Ji[1], Xiaorong Yue[1], Yuanyuan Jiang[1], and Zhaofei Li[1*]

[1]State Key Laboratory of Crop Stress Biology for Arid Areas, Key Laboratory of Northwest Loess Plateau Crop Pest Management of Ministry of Agriculture, College of Plant Protection, Northwest A&F University, Yangling 712100, China

[2]Key Lab of Integrated Crop Pest Management of Shandong Province, College of Plant Health and Medicine, Qingdao Agricultural University, Qingdao 266109, China

Running title: Domain IV of GP64 in membrane fusion

Keywords: baculovirus, AcMNPV, GP64, domain IV, viral fusion protein

Word count: Abstract, 250 words; Text, 7871 words.

*Corresponding author
Zhaofei Li
College of Plant Protection, Northwest A&F University,
Taicheng Road, Yangling 712100, China
Email: zhaofeili@nwsuaf.edu.cn
Tel: 86-18792598371

Abstract

Autographa californica multiple nucleopolyhedrovirus (AcMNPV) GP64 is a class III viral fusion protein that mediates low-pH triggered membrane fusion during virus entry. Although the structure of GP64 in a postfusion conformation has been solved, its prefusion structure and the mechanism of how the protein refolds to execute fusion are unknown. In postfusion structure, GP64 is composed of five domains (domain I-V). Domain IV (374-407 aa) contains two loops (loop 1 and loop 2) that form a hydrophobic pocket at the membrane-distal end of the molecule. To determine the roles of domain IV, we used alanine-scanning mutagenesis to substitute each of the residues and the contacts within domain IV and evaluate their contributions to GP64-mediated membrane fusion and virus infection. In many cases, substitution of a single amino acid has no significant impact on GP64. However, substitution of R392 or disrupting the contact N381-N385, N384-Y388, N385-W393, or K389-W393 resulted in poor cell surface expression and fusion loss of the modified GP64, whereas substitution of E390 or G391, or disrupting the contact N381-K389, N381-Q401, or N381-I403 reduced the cell surface level of the constructs and the ability of GP64 to mediate fusion pore expansion. In contrast, substitution of N407 or disrupting the contact D404-S406 appears to restrict fusion pore expansion without affecting expression. Combined with the identification of these constructs remaining stable prefusion conformation or dramatically less efficient transition from a prefusion to postfusion state under acidic conditions, we proposed that domain IV is necessary for refolding of GP64 during membrane fusion.

Importance

Baculoviruses GP64 is grouped with rhabdoviruses G, herpesviruses gB, and thogotoviruses glycoproteins as class III viral fusion proteins. In their postfusion structures, these proteins contain five domains (domain I-V). Distinguished from domain IV of rhabdoviruses G and herpesviruses gB that composed of β-sheets, domain IV of GP64 is a loop region and the same domain in thogotovirues glycorproteins has not been solved. In addition, domain IV is proximal to domain I (fusion domain) in prefusion structures of vesicular stomatitis virus (VSV) G and human cytomegalovirus (HCMV) gB but resides at the domain I-distal end of the molecule in a postfusion conformation. In this study, we identified that the highly conserved residues and the contacts within domain IV of AcMNPV GP64 are necessary for low-pH triggered conformational change and fusion pore expansion. Our results highlight the roles of domain IV of class III viral fusion proteins in refolding during membrane fusion.

1. Introduction

During infection, enveloped viruses enter into host cells via fusion of the virus envelope and cellular membranes (1). The virus-cell fusion reaction is catalyzed by one or more viral fusion proteins that are associated with the envelope of virus particles. Based on the characters of three-dimensional structures, viral fusion proteins have been classified into three distinct categories (class I-III) (2-4). Class I fusion proteins, such as hemagglutin (HA) of influenza virus, the coronaviruses spike (S) glycoprotein, and human immunodeficiency virus type 1 (HIV-1) GP41, are homotrimers and they are mainly consists of α-helix with a central coiled-coil. Class II fusion proteins, which include the E glycoprotein of flaviviruses and the E1 protein of alphaviruses, form an elongated homo- or heterotrimer mainly comprising of β-sheets with the internal fusion loops. Class III fusion proteins that include baculoviruses GP64, herpesviruses glycoprotein B (gB), the thogotoviruses glycoprotein (Gp), and the rhabdoviruses glycoprotein (G), share the structural features of both class I and class II proteins, such as the α-helical coiled-coil in the heart of homotrimers like class I and β-sheets holding the internal fusion loops like class II. Although viral fusion proteins from different classes show a great diversity in structural features, they appear to mediate fusion via a common mechanism (3). In a well-established stalk-hemifusion-pore model for biological membrane fusion, the fusion process mediated by viral fusion proteins undergoes several distinct stages. Initially, upon triggering by specific mechanisms (binding to cellular receptors and/or low-pH, etc.), the viral fusion proteins transit from the prefusion to postfusion structures and expose the fusion peptide or fusion loops, which insert into the target cellular membrane.

89 Then, refolding of the trimeric viral fusion proteins onto themselves brings the
90 host membrane into close proximity to the viral envelope. Following the two
91 separate membranes contact, merger of the outer membrane leaflets of the
92 membranes forms a hemifusion stage. Further refolding of the fusion proteins
93 into a stable postfusion structure drives the merger of inner leaflets of both
94 membranes to form fusion pore and subsequent fusion pore expansion to
95 release viral capsids into cells (3, 4).

96 Baculoviruses are enveloped, arthropod-specific viruses that are isolated
97 from the infected insects of the orders of Lepidoptera, Diptera, and
98 Hymenoptera. These viruses are composed of one or more rod-shaped
99 nucleocapsids that contain the circular double-stranded DNA genome
100 (approximately 80-180 kb) (5, 6). Baculoviruses are widely used as biological
101 pesticides in insect pest control and as vectors in protein expression and
102 mammalian cells transduction (5, 7, 8). *Autographa californica multiple*
103 *nucleopolyhedrovirus* (AcMNPV) is the archetype species of *Alphabaculovirus*
104 genus of the *Baculoviridae* family. In an infection cycle, AcMNPV replicates in
105 the nucleus and produces two kinds of virions with distinct phenotypes: the
106 occlusion-derived virions (ODVs) and budded virions (BVs). ODVs infect
107 midgut epithileal cells and may fuse with the plasma membrane of midgut cells
108 with the aid of the viral PIFs (*per os* infectivity factors) complex. BVs infect the
109 cells from other tissues and cells cultured *in vitro* (5, 9, 10). During entry, the
110 major envelope glycoprotein GP64 of AcMNPV BVs has receptor binding
111 activity and facilitates the attachment of BVs to the cell surface (11-13). Then,
112 BVs penetrate into cells via clathrin-mediated endocytosis (9, 10, 14, 15). In
113 the cellular endosomal system, low-pH triggers the conformational change of

GP64 mediated fusion of the envelope of BVs with endosomal membranes that leads to the release of nucleocapsids into the cytosol (16-18). In addition to its necessary roles in virus entry (receptor-binding and membrane fusion), GP64 is also required for nucleocapsids budding and release at the plasma membrane (19).

GP64 is a type I membrane protein that forms a disulfide-linked homotrimer and anchors at the apical and basal regions of AcMNPV BVs (18, 20, 21). Disruption of the intermolecular disulfide bond (C24-C372) of AcMNPV GP64 has a modest effect on the fusion activity (21). In determined structure of a low-pH (postfusion) form of AcMNPV GP64, the protein exhibits an extended conformation that is similar with those of other class III viral fusion proteins from herpesviruses, rhabdoviruses, and throgotoviruses (18, 22, 23). Currently, vesicular stomatitis virus (VSV) G is the only class III fusion protein which prefusion and postfusion structures have been solved in high resolutions (24, 25). In low-pH triggered conformational change, the prefusion to postfusion states transition of VSV G may adopt monomeric stages with the individual domains may retain their structures (25-27). However, the detailed molecular mechanisms of the conformation change of class III viral fusion proteins are not clear.

In its postfusion structure, GP64 is composed of five domains (domains I-V) (18). Domain I resides at the base of the molecule closing to the membrane or viral envelope (18). This domain contains two fusion loops (loop 1 and 2) in which the hydrophobic residues are essential for membrane interaction and the progression of distinct stages of membrane fusion (17, 28). At the opposite end of the molecule (top end), domain IV (residues 374-407) connects the

central α-helical domain III and the C-terminal domain V (18) (Fig. 1A). Different from domain IV of herpesviruses gB and VSV G that are made entirely of β-sheets, domain IV of GP64 is a loop region in which few residues (394-398 aa) have not been solved in the structure (18, 24, 29, 30). Similarly, in thogotoviruses (Thogoto virus, Dhori virus, and Bourbon virus) glycoproteins (Gps), domain IV has not been solved in their postfusion structures (23, 31). In the prefusion structure of VSV G and a recently determined low resolution prefusion structure of human cytomegalovirus (HCMV) gB, domain IV is close to domain I (the fusion domain that contains fusion loops) (25, 32). The conformational changes of VSV G and HCMV gB from prefusion to postfusion structures may rearrange domain IV to the top end of the trimer distant from domain I and the membrane (26, 32). The biological functions of domain IV of class III viral fusion proteins are not clear. In this study, to investigate the roles of domain IV in membrane fusion, we made substitutions of the individual residue and residues that form contacts within domain IV of AcMNPV GP64 with alanine and analyzed the effect of these mutations on the ability of GP64 to mediate membrane fusion. The modified *gp64* genes were also introduced into a *gp64* knockout AcMNPV bacmid and their effects on virus infection were assessed in transfected and infected cells.

Results

Domain IV of GP64 shields the top end of domain III to form a hydrophobic pocket

To determine the roles of domain IV of GP64, we first performed an analysis of the postfusion structure of GP64 (PDB, ID: 3DUZ) (18) by using WHAT IF molecular modeling package (http://swift.cmbi.ru.nl/whatif/) and I-TASSER

(Iterative Threading ASSEmbly Refinement) approach (33) to identify the potential amino acid side-chain contacts among residues within domain IV or the contacts between residues within domain IV and residues from other domains. In the postfusion structure of GP64, domain IV is located at the membrane-distal end of the molecule and close to the top end of domain III (Fig. 1A, B). This domain is composed of two adjacent loops that connected by a conserved disulfide bond (C382-C402) (21) (Fig, 1C, D). At the top of the structure, two loops of domain IV fold back as a lid structure toward the center of the molecule and shield the top end of the α-helix of domain III to form a hydrophobic pocket (Fig. 1C). Within the pocket, the conserved YxEGRW motif (Y388-x-E390-G391-R392-W393) is located at the tip of the lid structure, whereas the conserved hydrophilic, hydrophobic, and charged residues T379, N381, N384, N385, Y388, K389, W393, I401, Q403, and F405 within domain IV form complex network contacts within loop 1 or between two loops, including T379-F405, N381-N385, N381-K389, N381-I401, N381-Q403, N384-Y388, N385-K389, N385-W393, and K389-W393. In addition, at the lateral side of loop 2, D398 forms contacts with S400 and Q401, and D404 forms a contact with S406 (Fig. 1C, D). All these contacts occur in the same monomer of GP64. Sequence alignment indicated that the residues involved in the interactions are highly conserved in GP64 proteins from different baculoviruses and in the GP64-family homologs from thogotoviruses (Fig. 1E). Based on structural analysis of AcMNPV GP64 and sequence conservation among the GP64 family proteins, we used site-directed mutagenesis to individually mutate the conserved residues to alanine or mutate the interacting residues in pair to alanines and assessed the contribution of each residue or

interaction to GP64 function (Table 1). Note that, in predicted structures of domain IV, individual alanine-substitution of T379, N381, N384, N385, K389, Q401, or I403 did not disrupt the original paired interactions mediated by these residues (Table 1).

Substitution of the YxEGRW motif or disrupting the contacts in domain IV affects cell surface expression and localization of GP64

To examine the effect of alanine-substitution on GP64 expression and cell surface localization, Sf9 cells were transfected with the plasmid transiently expressing wild-type (WT) or modified GP64 proteins under the control of the promoter of the AcMNPV *ie1* gene. At 36 h post-transfection (p.t.), GP64 proteins in cell lysates were separated by reducing or non-reducing SDS-PAGE and then detected by Western blotting. Under non-reducing conditions, GP64 monomers are covalently linked by intermolecular disulfide bonds to form trimers. As shown in Figure 2A, the similar trimer forms (trimer I and trimer II) that are typically observed for WT GP64, were detected from all GP64 proteins containing substitutions. For most of the substituted GP64 constructs, the size and intensities of bands corresponding to the WT and modified GP64 proteins were similar, suggesting that the substitution did not substantially alter the expression or oligomerization of those GP64s. Similar with that observed previously (34), single substitution of the *N*-glycosylation site N385 (N385A) or mutation of the paired residues containing N385 (N381/N385A, N385/K389A, and N385/W393A) resulted in a slight reduction of the molecular weight (MW) of the modified GP64s. In addition, disrupting the interaction of T379-F405 (F405A and T379/F405A) resulted in a slight increasing of the MW of the modified proteins on either reducing or

214 non-reducing gels (Fig. 2 A). A possible interpretation is that substitution of
215 F405 or T379 and F405 for alanine may alter the local hydrophobicity of the
216 modified proteins and reduce the amount of SDS binding to the proteins on
217 SDS-polyacrylamide gels.

218 Cell surface expression of the GP64 constructs was assessed by using a
219 cell surface enzyme-linked immunosorbent assay (cELISA) and compared to
220 that detected from WT GP64 (Fig. 2B). Of the 29 single-alanine substitution
221 mutations examined, cell surface level for 20 of them was nearly similar with
222 that of WT GP64, and that for the other 4 constructs (N381A, Y383A, N384A,
223 and N385A) was reduced 23.7-46.7%. In contrast, severe reduction of the cell
224 surface level was detected for constructs with substitutions in 5 highly
225 conserved amino acid positions (Y388A, E390A, G391A, R392A, and W393A).
226 Similarly, poor cell surface expressions were also observed for 5 of the 12
227 double-alanine substitution constructs (N381/N385A, N381/K389A,
228 N384/Y388A, N385/W393A, and K389/W393A) (Fig. 2B, C, Table 1).

229 To confirm the cell surface localization of the GP64 constructs with poor cell
230 surface expression (below 20% of that from WT GP64), the transfected Sf9
231 cells expressing the WT or modified GP64 were examined using indirect
232 immunofluorescence with the monoclonal antibody (MAb) AcV1 that
233 recognizes the native neutral-pH conformation (prefusion form) of GP64 (35).
234 The results indicated that the GP64 proteins were present at the surface and
235 AcV1 binding indicated that they were in the native prefusion conformation
236 (data not shown). Together, these results suggest that the YxEGRW motif and
237 the intramolecular contacts network mediated by N381, N384, N385, Y388,
238 K389 or W393 are critical for cell surface localization of GP64 (Fig. 2C).

Substitution of the YxEGRW motif or disrupting the contacts in domain IV restricts membrane fusion

To determine whether mutations in domain IV affect membrane fusion, we first evaluated the fusion activities of WT and the modified GP64s in a cell-cell fusion assay. Because the cell surface level of GP64 is correlated with its fusion activity and cell surface levels varied among different modified GP64 constructs, we initially established a standard curve for cell surface level and fusion activity of WT GP64 by transfecting Sf9 cells with decreasing quantities (0.005-2 μg) of the plasmid expressing WT GP64 (Fig. 2B, left side of the panel, data not shown). The fusion (syncytium formation) activity of each modified GP64 construct was determined and then normalized with that from WT GP64 that was localized to the cell surface at an equivalent level. Most of the substitution constructs including four of them with a significant reduction of cell surface expression (N381A, Y383A, N384A, and N385A) mediated WT levels or a minor reduction level of fusion (Figs. 2B, 3A, B). In contrast, single substitution of the YxEGRW motif, D404 or N407, or the paired substitutions (N381/N385A, N381/K389A, N381/Q401A, N381/I403A, N384/Y388A, N385/K389A, N385A/W393A, K389/W393A, and D404/S406A) that disrupting the contacts formed by N381, N384, N385, Y388, K389, W393, Q401, I403, D404, and S406 resulted in loss or dramatic reduction of fusion activity of modified GP64 proteins (Fig. 3). Those constructs that impaired fusion activity of GP64 can be further classified as three groups: i) The constructs D404A, N407A, and D404/S406A were expressed at the cell surface with nearly WT levels, but only induced few and small syncytia and maintained substantially low fusion activity (Figs. 2B, 3). ii) Two constructs N381/Q401A and

264 N381/I403A were localized at the cell surface with a significantly low level, and
265 their normalized fusion efficiencies were reduced to 7.6-11.0% (Fig. 3, Table 1).
266 iii) The constructs Y388A, E390A, G391A, R392A, W393A, N381/N385A,
267 N381/K389A, N384/Y388A, N385/W393A, and K389/W393A have poor cell
268 surface localization and no detectable fusion activity (Figs. 2B, 3, Table 1).

269 To further determine in which step the membrane fusion was restricted for
270 the GP64 constructs with impaired fusion activity, we used a dye-transfer
271 assay to detect hemifusion (outer membrane leaflet merger) and pore
272 formation (inner leaflet merger) by observing the transfer of a
273 membrane-specific dye (lipophilic octadecyl rhodamine B chloride, R18) and a
274 cytosolic dye (calcein-AM) between red blood cells (RBCs) and Sf9 cells as
275 described in prior studies (17, 36). In this assay, RBCs were dual-labeled with
276 R18 and calcein-AM, then attached to Sf9 cells that expressing WT or the
277 modified GP64. After triggering under low-pH conditions, the transfer of each
278 dye between RBCs and Sf9 cells was observed and dye transfer efficiencies
279 were calculated. Based on the dye-transfer efficiencies, the membrane fusion
280 defect for constructs of GP64 can be classified as either: a) inhibiting outer
281 membrane leaflet merger (hemifusion) or b) reducing the efficiency of pore
282 formation or expansion (Fig. 4A). As shown in Figure 4B, no dye transfer
283 (neither R18 nor calcein-AM) was observed for the constructs Y388A, E390A,
284 G391A, R392A, W393A, N381/N385A, N381/K389A, N384/Y388A,
285 N385/W393A, and K389/W393A. This suggests that either substitution of the
286 residues at the YxEGRW motif or substitutions that disrupting the contacts
287 formed by N381, N384, N385, Y388, K389, and W393 impaired the ability of
288 GP64 to catalyze the initial merger of the outer membrane leaflets. For

289 constructs D404A, N407A, N381/Q401A, N381/I403A, and D404/S406A that
290 showed a substantial reduction of fusion activity (Fig. 3), they appear to impair
291 membrane fusion at a distinct step. For these constructs, we observed the
292 transfer of both R18 and calcein-AM dyes between RBCs and Sf9 cells (Fig.
293 4B), and dye transfer efficiencies were relatively high, ranging from 64.2% to
294 83.8% (Fig. 4C). Thus, constructs D404A, N407A, N381/Q401A, N381/I403A,
295 and D404/S406A induced complete fusion pores formation, but the fusion pore
296 may not be efficiently expanded. Combined, these results suggest that, while
297 most of the residues in domain IV were not necessary for membrane fusion
298 activity of GP64, the YxEGRW motif (Y388-x-E390-G391-R392-W393), N407,
299 and the contacts formed by N381, N384, N385, Y388, K389, W393, Q401,
300 I403, D404, and S406 were critical for initial membrane merger or fusion pore
301 expansion.

302 **Substitution of the YxEGRW motif or disrupting the contacts in domain**
303 **IV alters the conformational change of GP64**

304 To determine whether the membrane fusion defect for those constructs that
305 could not induce hemifusion and fusion pore expansion was resulted from a
306 detectable effect on the low-pH triggered conformational change in GP64, the
307 binding of a conformation-specific MAb AcV1 on the cell surface was examined
308 by cELISA under various pH conditions (Fig. 5). As known, the AcV1 antibody
309 recognizes only the neutral-pH (or prefusion) conformation of GP64, and that
310 the AcV1 epitope is lost upon the low-pH triggered conformational change (35).
311 To monitor the potential change of the cell surface level for each GP64
312 construct corresponding to low-pH treatment, the transfected cells expressing
313 WT or modified GP64 proteins were also analyzed by cELISA with the MAb

AcV5, which binds to the denatured GP64 (37). As expected, treatment of the transfected cells with successively decreasing the pH of PBS from 7.0 to 4.5 did not significantly change the cell surface level of WT or each modified GP64 (data not shown). Low-pH treatments resulted in a dramatic lose of AcV1 binding to WT GP64 (Fig. 5, WT). For the modified GP64, the binding activity of AcV1 under various pH conditions could be subdivided into three categories: i) The constructs (Y388A, E390A, G391A, R392A, W393A, N381/N385A, N381/K389A, N384/Y388A, N385/W393A, and K389/W393A) that were detected with significantly low level at the cell surface using the MAb AcV5 (Fig. 2B, data not shown) showed significantly low binding to AcV1 at neutral-pH or higher low-pH conditions. However, the binding activities of AcV1 for these constructs appear to increase substantially after treatment with PBS at pH 4.5 (Fig. 5A, B). ii) Two constructs N381/Q401A and N381/I403A that were present at the cell surface with a dramatically low level (Fig. 2B, data not shown) showed relatively high AcV1-binding activities at neutral-pH conditions and loss of AcV1 binding at various low-pH values (Fig. 5C). iii) Three modified GP64 constructs D404A, D404/S406A, and N407A that were expressed at the cell surface at a similar level as WT GP64 (Fig. 2B, data not shown) also showed WT or a minor low levels of AcV1-binding activities at neutral-pH conditions (Fig. 5D). Upon low-pH trigger, these constructs showed a very modest pattern of loss of AcV1-binding as pH values were lowered from 7.0 to 5.0. Even after treatment with PBS at pH 4.5, the AcV1-binding activities of these constructs were significantly higher than that of WT GP64 (Fig. 5D). These results suggest that even though membrane fusion is affected at two distinct stages for different sets of constructs (Fig. 4), the low-pH triggered

conformational change appears to be dramatically affected in both cases. Thus, these mutations (except that of N381/Q401A and N381/I403A) may alter the neutral-pH conformation of GP64 and generate the structural or energy obstacle (Note: The refolding of the modified proteins from a prefusion to a postfusion conformation may require higher energy) to prevent the low-pH triggered prefusion to postfusion conformational change of the modified GP64.

Substitution of the YxEGRW motif or disrupting the contacts in domain IV affects infectious virus production

To determine whether introduction of alanine in domain IV to substitute a specific amino acid or paired residues affect infectious AcMNPV production, we constructed recombinant AcMNPV bacmid expressing WT or each modified GP64 under the control of the native promoter of AcMNPV *gp64* gene. At 96 h p.t., the cell culture supernatants were used to infect Sf9 cells. At 96 h post-infection (p.i.), the infectious virus titers were determined and the infectious BVs production for the recombinant viruses that expressing modified GP64 proteins with no significant or a minor reduction of fusion activities was similar with that of the virus expressing WT GP64 (Table 1). For constructs (D404A, N407A, N381/Q401A, N381/I403A, and D404/S406A) with dramatic reduction of fusion activities (Figs. 3, 4), we also observed a WT level of infectious virus production (Table 1). In contrast, no measurable infectious BVs were detected for each of the constructs expressing Y388A, R392A, W393A, N381/385A, N384/Y388A, N385/W393A, or K389/W393A (Table 1). It is expected that those modified GP64 proteins could not induce membrane fusion (Figs. 3, 4). However, infectious BVs with about 30-180 fold reduction of production were detected for the construct expressing E390A, G391A, or

364 N381/K389A that inhibit membrane fusion in a cell-cell fusion assay (Figs. 3, 4,
365 Table 1).

366 To further assess the potential effect of the modified GP64 proteins with
367 impaired fusion activities on infectious BVs generation, we performed one-step
368 and multistep virus growth curve analyses to evaluate virus replication kinetics.
369 As shown in Figure 6A, no significant difference of infectious BVs production
370 was observed for viruses expressing the modified GP64 protein D404A,
371 N407A, N381/Q401A, N381/I403A, or D404/S406A or WT GP64 at any time
372 points p.i.. In contrast, the infectious virus production for $V^{N381/K389A}$ at each
373 time point p.i. in both growth curves were significantly lower than that for the
374 virus expressing WT GP64 (Fig. 6B). Similar but with a more dramatic
375 reduction of virus production were observed for V^{E390A} and V^{G391A} (Fig. 6B).
376 Thus, substitution of D404 or N407, or mutations disrupting the contacts
377 N381-Q401, N381-I403, or D404-S406 had no apparent effect on infectious
378 BVs production. Rescue the *gp64* knockout virus infectivity by E390A, G391A,
379 or N381/K389A, even though with a substantial low rate, suggests that these
380 constructs may properly fold to perform conformational change and restore the
381 fusion activity in virus-infected cells.

382 **Constructs E390A, G391A, and N381/K389A restore membrane fusion in**
383 **virus-infected cells**

384 Because constructs E390A, G391A, and N381/K389A that inhibited
385 hemifusion in transiently expressing cells rescue the infectivity of *gp64*
386 knockout AcMNPV, we asked whether these proteins could induce membrane
387 fusion in virus-infected cells. To examine this question, Sf9 cells were infected
388 with the virus expressing E390A, G391A, N381/K389A, or WT GP64 and then

the expression and fusion activity of these proteins were examined. As shown in Figure 7, these constructs were expressed and oligomerized into trimers as WT GP64 (Fig. 7A). The cell surface levels for these modified GP64s were ranged from 25.2-34.4%, dramatically lower than that of WT GP64 (Fig. 7B). Membrane fusion analysis showed that E390A, G391A, and N381/K389A could only induce a few syncytia in virus-infected cells and the percentage of cells in syncytia for these constructs were about only 5.5-12.8% (Fig. 7C, D).

To dissect in which step the membrane fusion activity for the modified GP64s were impaired, we used the dye-transfer assay as mentioned above to detect hemifusion and pore formation induced by these constructs in virus-infected cells. As shown in Figure 7E, we observed both of the membrane and cytosolic dyes (R18 and calcein-AM) transfer between RBCs and infected Sf9 cells induced by E390A, G391A, and N381/K389A under low-pH conditions (pH 5.0), even though the dye transfer efficiencies for these proteins were significantly low in comparison with that of WT GP64 (Fig. 7F). Using the MAb AcV1, we also analyzed the antibody-binding activity for each of the constructs under various pH conditions (pH 7.0-4.5). The results showed that, in comparison with the loss of AcV1-binding activity for WT GP64 response to low-pH treatments, the AcV1-binding activity of E390A, G391A, or N381/K389A substantially low at neutral-pH conditions, and the binding activities for these constructs were not affected upon low-pH treatment at pH 5.7 but decreased slightly corresponding to more acidic treatments (pH 5.5-4.5). It is worth noting that the AcV1-binding activities for E390A, G391A, and N381/K389A at pH 4.5 were significantly higher than that for WT GP64 (Fig. 7G). cELISA analysis with the MAb AcV5 indicated that the cell surface

level for these proteins were not significantly changed upon various pH treatments (pH 7.0-4.5) (data not shown). Together, these results indicate that, upon low-pH trigger, E390A, G391A, and N381/K389A may partially refold from the prefusion to postfusion states and induce membrane fusion in a low efficiency in virus-infected cells.

Constructs E390A, G391A, and N381/K389A affect virus entry but not egress

Since the constructs E390A, G391A, and N381/K389A could induce membrane fusion in virus-infected cells (Fig. 7), we next asked whether the impaired fusion activity for these proteins has a negative effect on either virus binding to or penetration into cells, or progeny virus egress, and that in turn may result in slow virus growth kinetics (Fig. 6). First, Sf9 cells were incubated with the purified virus expressing WT or modified GP64 proteins at low-temperature and then the cell-binding efficiency of each virus was determined by measuring of the virus genomic DNA using quantitative real-time PCR (qPCR) (Fig. 8A, panel a). As shown in Figure 8A, in comparison with the control (V^{WT}-GFP), the binding efficiency of each of the virus V^{E390A}-GFP, V^{G391A}-GFP, and $V^{N381/K389A}$-GFP was similar with that of V^{WT}-GFP, suggesting that mutation of E390, G391, or N381-K389 has no apparent effect on virus binding (Fig. 8A, panel b). To further determine virus entry, Sf9 cells were incubated with the purified virus at 4°C for binding. Then, the culture temperature was raised to 27 °C to allow the virus to internalize into cells. At 1 h post-internalization, any virions remaining at the cell surface were inactivated and removed by treatment with citrate buffer (pH 3.1) as described in prior studies (15). The cells were used to extract total DNA and viral genomic

439 DNA was quantified by qPCR. As shown in Figure 8A, the amount of
440 internalized viruses of V^{E390A}-GFP, V^{G391A}-GFP, or $V^{N381/K389A}$-GFP were
441 significantly lower than that of V^{WT}-GFP (Fig. 8A, panel c). Together, these
442 results suggest that single substitution of E390 or G391, or disrupting the
443 contact N381-K389 affect the efficient entry of BVs.

444 Since GP64 is necessary for efficient budding and release of progeny
445 nucleocapsids (19), we next examined whether E390A, G391A, and
446 N381/K389A affect virus egress. To circumvent the negative effect of these
447 constructs on virions entry, we transfected Sf9 cells with recombinant AcMNPV
448 bacmids encoding WT or the modified GP64 and two reporters (GFP and
449 β-glucuronidase (β-Gluc)). The cell surface level of GP64s and infectious virus
450 production were determined at a narrow time period after transfection (24 h p.t.)
451 (Fig. 8B, panel a). Also, the GFP fluorescence and β-Gluc activity were
452 measured (at 24 h p.t.) to ensure that transfection efficiencies and initiation of
453 infection by the different bacmids were equivalent. At 24 h p.t., the percentage
454 of GFP-positive cells in transfections with the same amount of DNA (4 μg/well)
455 for the different bacmids (V^{WT}-GFP, V^{E390A}-GFP, V^{G391A}-GFP, and
456 $V^{N381/K389A}$-GFP) was ranging from 30.1-32.5%, and the activities of β-Gluc in
457 cell lysates from the different bacmids transfected cells were similar (data not
458 shown), suggesting that transfection efficiencies were equivalent for all
459 bacmids and that in each case the bacmid initiated an infection that
460 progressed into the late phase of the infection cycle. Since the cell surface
461 level of E390A, G391, and N381/K389A were significantly lower than that of
462 WT GP64 in plasmids-transfected cells or in virus-infected cells (Figs. 2, 7), we
463 generated a range of decreasing GP64 cell surface levels by transfecting Sf9

464 cells with decreasing quantities of the bacmid that expresses WT GP64 (Fig.
465 8B, panel b). In bacmid-transfected cells, the cell surface levels for E390A,
466 G391A, and N381/K389A were reduced by approximately 62.3-78.4% and a
467 similar reduction was observed from transfection with 0.5 μg or 1.0 μg of the
468 bacmid expressing WT GP64 (Fig. 8B, panel b). Infectious BVs production was
469 then measured from the same transfected cells (Fig. 8B, panel c).
470 Comparisons of virus production in cells expressing the modified GP64s with
471 that from WT GP64-expressing cells (in which the cell surface levels of GP64
472 were similar; see dashed lines in Fig. 8B, panels b and c), showed that there
473 was no significant reduction of infectious BVs production in cells expressing
474 either E390A, G391A, or N381/K389A when compared with BVs produced
475 from cells expressing a similar level of WT GP64 (Fig. 8B, panel c). Together,
476 these results suggest that the constructs E390A, G391A, and N381/K389A
477 affect efficient virus entry but not egress of progeny BVs.

478 **Discussion**

479 During the entry of enveloped viruses, fusion of the viral envelope and
480 cellular membrane that mediated by viral fusion proteins is required for delivery
481 of viral genome into host cells (1, 3, 4). Based on the determined postfusion
482 structure, GP64 is grouped with herpesviruses gB, rhabdoviruses G, and
483 throgotoviruses Gps as class III viral fusion proteins (18, 22, 23, 26). In its
484 postfusion structure, GP64 is composed of five domains (18). Domain IV is
485 located at the membrane-distal end of the molecule and coordinated with the
486 top end of domain III to form a hydrophobic pocket (Fig. 1). Prior studies
487 showed that the disulfide bond C382-C402 in domain IV of GP64 is essential
488 for the protein stability (21). In the current study, we extended the observation

by using site-directed mutagenesis to demonstrate that the intramolecular contacts (N381-N385, N381-K389, N381-Q401, N381-I403, N384-Y388, N385-W393, K389-W393, and D404-S406), a cluster of Y388-x-E390-G391-R392-W393 motif and the C-terminal N407 in domain IV of AcMNPV GP64 are critical for low-pH triggered conformational change and fusion pore expansion during membrane fusion.

In alanine-scanning mutagenesis, single substitution of N407 or disrupting the contact D404-S406 has no significant effect on the cell surface expression of the modified GP64s, but resulted in a dramatic reduction of fusion activities. Dye-transfer assays indicated that these substitutions could efficiently induce fusion pore formation but appear to defect in fusion pore expansion (Fig. 4). D404, S406, and N407 reside at the C-terminus of domain IV and connect with the loop region of domain V (Fig. 1). Prior studies indicated that the interaction of the loop region of domain V with the central coiled-coil in domain III of herpes simplex virus 1 (HSV-1) gB promotes the gB structure transition to a postfusion conformation (38). In response to low-pH trigger, the constructs D404A, D404/S406A, and N407A showed a dramatically less efficient transition from prefusion to postfusion states (as detected by AcV1 binding) (Fig. 5), suggesting that the contact D404-S406 and N407 may play a role in low-pH triggered conformational change of GP64.

Similarly, the contact network formed by N381, N385, K389, Q401, and I403 (N381-N385 and N381-K389 in loop 1, N381-Q401 and N381-I403 between loop 1 and loop 2) at the middle region of domain IV was also identified as playing roles in refolding or stability of GP64. Double-alanine substitution of N381 and Q401 or N381 and I403 has a dramatic effect on

514 fusion activities of the modified GP64s. Both constructs (N381/Q401A and
515 N381/I403A) underwent low-pH triggered conformation change and induced
516 pore formation, but seems to be defective in fusion pore expansion (Fig. 4). In
517 domain IV, the contacts N381-Q401 and N381-I403 surround the
518 intramolecular disulfide bond C382-C402 (Fig. 1D), which is essential for GP64
519 folding and stability (21). In the well-established hemifusion-pore membrane
520 fusion model, low-pH or other mechanisms triggered conformational change
521 promotes the fusion peptide or fusion loops of viral fusion proteins insert into a
522 target membrane. Then, the fusion proteins fold back toward themselves and
523 form energy-stable postfusion structures to drive fusion pore expansion (3, 4).
524 The negative effect of disrupting one of the two contacts (N381-Q401 and
525 N381-I403) on GP64-mediated fusion may be interpreted as the substitution
526 attenuating or destabilizing the disulfide bond C382-C402, and which in turn
527 affect the modified proteins refolding or stability. For another two constructs
528 N381/N385A and N381/K389A, the mutations resulted in the membrane fusion
529 defect at the initial stage (hemifusion). Low-pH treatments appear to alter the
530 prefusion structure of these modified GP64s (Fig. 5A), suggesting that the
531 contact N381-N385 and N381-K389 play a role in transition of prefusion to
532 postfusion states. Surprisingly, the virus expressing N381/K389A was able to
533 replicate, although very inefficiently in producing infectious BVs. In infected
534 cells, N381/K389A induced few syncytia formation. It seems that, in infected
535 cells, N381/K389A may undergo partially proper folding, induce fusion pore
536 formation but affect pore expansion. The impact of N381/K389A on virus entry
537 but not on virus egress further suggests the roles of N381-K389 in membrane
538 fusion.

539 In addition to form the necessary contacts N381-N385 and N381-K389 in
540 loop 1, the residues N385 and K389 also form contacts with W393, which
541 resides at the bottom of loop 2 in domain IV (Fig. 1D). Disruption of these
542 contacts (W393A, N385/W393A, or K389/W393A) resulted in low expression
543 of the modified GP64 at cell surface and the defect of membrane fusion.
544 Modeling structure analyses indicated that disrupting the contact N385-W393
545 or K389-W393 resulted in the top region of loop 2 shifted to the center of the
546 molecule about 2.5 Å and a shift of the backbone and side chains of
547 E390-G391-R392 which reside at the base of loop 1 towards outside of the
548 molecule about 2 Å (data not shown), suggesting that the contacts N385-W393
549 and K389-W393 are critical for maintaining the conformation of domain IV.
550 Similar with the negative effect observed for these constructs, disruption of the
551 contact N384-Y388 at the top region of loop 1 (Y388A or N384/Y388A) or
552 single substitution of E390, G391, or R392 also caused a dramatic reduction of
553 cell surface level of the modified GP64 and the defect of membrane fusion at
554 the initial stage (hemifusion) (Figs. 2-4). For all these constructs, low-pH
555 trigger seems to alter the prefusion conformation (Fig. 5A), suggesting that the
556 contacts N384-Y388, N385-W393, and K389-W393, and E390, G391, and
557 R391 also play a role in conformational change of GP64.

558 Similar with that observed for N381/K389A, viruses expressing E390A or
559 G391A also replicated inefficiently. The defect of virus replication seems to
560 result from the reduced efficiency of virus entry (Fig. 8A). Although these two
561 constructs also underwent low-pH triggered conformational change in
562 virus-infected cells, the significantly slow decreasing of AcV1-binding activities
563 under low-pH conditions suggests they have a role in conformational change

564 of GP64. In addition, in postfusion structure of GP64, E390-G391-R392 is
565 located at the tip of the lid structure of the hydrophobic pocket and form the
566 turn between loop 1 and loop 2 (Fig. 1C, D). Previous studies have
567 demonstrated that Arginine-Glycine-Aspartic acid (RGD) motif in some vial
568 proteins binds integrin to promote virus entry or activate the integrin signal
569 pathway to facilitate the intracellular trafficking of viral proteins (39). Intriguingly,
570 substitution of E390 with aspartic acid (E390D) has no effect on the expression
571 and fusion activity of the modified GP64 and virus infection, whereas
572 substitution of R392 with histidine or lysine (R392H or R392K) abolished the
573 cell surface expression and fusion activity of GP64 (data not shown). The
574 receptor-binding domain of GP64 has been mapped within the N-terminal 160
575 aa (12). Therefore, the conserved EGR motif of GP64 (in thogotoviruses Gps
576 as DGR) may be unrelated with the plasma membrane binding of GP64, but
577 may mediate the interaction of GP64 with some cellular factors (such as
578 integrin) to promote the trafficking of GP64 to the cell surface or proper folding.
579 In class III viral fusion proteins, VSV G is the only protein for which the high
580 resolution structures of prefusion and postfusion states have been solved (24,
581 25). In low-pH triggered conformational change of VSV G, the prefusion to
582 postfusion structures transition proceeds through monomeric stages of G with
583 the domains mostly retain their structures (26, 27). A similar conformational
584 change may be adopted by herpesviruses gB according to a recently
585 determined low resolution prefusion structure of HCMV gB (32). In the
586 prefusion structures of VSV G and HCMV gB, domain IV are located at the
587 lateral side of the molecules and proximal to the middle or upper regions of
588 domain I, which contains fusion loops. However, in postfusion structures,

589 domain IV in both proteins is rearranged to the top end of the molecule and
590 distal from domain I that resides at the bottom of the molecule (24, 25, 32, 40).
591 Structural comparison and phylogenetic analyses suggest that the class III
592 viral fusion proteins have evolved from a common ancestor (23). In addition,
593 although class III viral fusion proteins from different viral families exhibit distinct
594 characters in activation and interaction with the target membrane, they share
595 the similar molecular architecture in the postfusion state (23, 26). Intriguingly,
596 the negative effect of mutations in domain IV on membrane fusion (i.e. defect
597 in hemifusion and fusion pore expansion) in the current study is similar with
598 that observed in prior studies for mutations in fusion loops of AcMNPV GP64
599 (17, 28). Based on the prefusion structure of VSV G (25), we generated a
600 predicted prefusion structure of GP64 using I-TASSER approach (Fig. 9A) (33)
601 and proposed a model of roles of domain IV in the prefusion to postfusion
602 conformational change of GP64 (Fig. 9B). In this model, we hypothesize that in
603 neutral-pH conditions, the cell surface or viral envelope localized GP64 may
604 adopt a compact prefusion conformation, in which domain IV may be proximal
605 to domain I. Upon low-pH trigger, domain I extends outside and exposes fusion
606 loops that interact with the target membrane. Followed with the long central
607 coiled-coil formation in domain III (and may be the interaction of domain III, IV,
608 and V) and the extension of domain V, domain IV is pushed to the top end of
609 the molecule. These structure rearrangements bring two membranes close to
610 fusion (Fig. 9B).

611 In conclusion, we examined the functional roles of domain IV in baculovirus
612 GP64-mediated membrane fusion. Each of the intramolecular contacts and
613 residues within domain IV was analyzed for their effects on GP64-mediated

membrane fusion and virus infection. The intramolecular contacts formed by the conserved residues N381, N384, N385, Y388, W393, Q401, I403, D404, and S406, a cluster of residues Y388-x-E390-G391-R392-W393 that made the turn between loop 1 and loop 2, and N407 at the C-terminus of domain IV were identified as important for low-pH triggered conformational change and/or fusion pore expansion of GP64. These data will be more definitively fit into the structure transition when the prefusion conformation of GP64 becomes available and highlight the refolding mechanism of class III viral fusion proteins during membrane fusion.

Materials and methods

Cells and transfections

Spodoptera frugiperda Sf9 cells were grown in TNMFH medium (Sigma-Aldrich) supplemented with 10% fetal bovine serum (Gibco) and maintained at 27 °C. Cells in 6-well plates (1×10^6 cells per well) or 12-well plates (2×10^5 cells per well) were transfected with plasmids or bacmids DNA using a $CaPO_4$-precipitation method (16).

Mutagenesis and construction of plasmids and bacmids

Site-directed mutagenesis was performed with overlap PCR. The C-terminal 882 bp fragments of AcMNPV *gp64* encoding substitution mutations were amplified using pBiepA (36) as the template. PCR products were digested with NotI and EcoRI, and then inserted into pBiepA to generate the plasmid P*ie1*-XpBlue (X represents a specific mutation of GP64). To generate AcMNPV bacmids encoding the substitution construct of GP64, the promoter of AcMNPV *gp64* was amplified by PCR using the bacmid DNA and then digested with SacI and XbaI and inserted into GFPpFB (41) to generate the

639 plasmid P*gp64*-GFPpFB. Then, the fragment encoding WT or the modified
640 GP64 that isolated from pBiepA or P*ie1*-XpBlue with XbaI and EcoRI were
641 separately inserted into P*gp64*-GFPpFB to generate the pFastbac plasmid
642 P*gp64*-XpFB. To generate AcMNPV bacmids expressing certain construct of
643 GP64 (WT, E390A, G391A, or N381/K389A) and GFP, a cassette containing
644 the AcMNPV *ie1* promoter, *gfp*, and the poly(A) sequence of AcMNPV *gp64*
645 were isolated from GFPpBlue (42) with KpnI and HindIII and inserted into
646 P*gp64*-XpFB to generate the pFastbac plasmid P*gp64*-X-P*ie1*-GFPpFB. The
647 resulting pFastbac constructs were each cloned into the *polyhedrin* locus of an
648 AcMNPV *gp64*-null bacmid (19) by Tn*7*-mediated transposition (43). All
649 constructs were verified by DNA sequencing. The plasmid and bacmid DNAs
650 used for transfection were isolated with the Hipure Midiprep kit (Invitrogen).

651 **cELISA**

652 The cell surface-localized GP64 proteins were detected using cELISA as
653 previously described (36). Briefly, Sf9 cells in 12-well plates were transfected
654 with the plasmid expressing WT GP64 or the modified GP64 or infected with
655 the virus expressing WT or modified GP64 proteins. At 36 h p.t. or 48 h p.i., the
656 cells were fixed with 0.5% glutaraldehyde and relative levels of cell
657 surface-localized GP64 were detected by using anti-GP64 MAb AcV5 (Santa
658 Cruz Biotechnology), the goat anti-mouse IgG conjugated with β-galactosidase
659 (SouthernBiotech), and the substrate chlorophenolred-β-D-galactopyranoside
660 (CPRG, Roche Life Science). To determine the low-pH-triggered
661 conformational change of the cell surface-localized GP64 proteins, cELISA
662 was performed with anti-GP64 MAb AcV1 (Santa Cruz Biotechnology). For this
663 assay, transfected or infected Sf9 cells (at 36 h p.t. or 48 h p.i.) were incubated

664 in PBS adjusted to different pH values (4.5 to 7.0) for 20 min, and then fixed
665 with 2% paraformaldehyde for 30 min. The following steps in cELISA were
666 similar to those used for the MAb AcV5.

667 **Immunofluorescence analysis**

668 Sf9 cells in 12-well plates were transfected with 2 μg of the plasmid
669 expressing WT or the modified GP64. At 36 h p.t., the cells were fixed with 2%
670 paraformaldehyde for 30 min. The cell-surfaced localized GP64 proteins were
671 visualized by indirect immunofluorescence using the MAb AcV1 and Alexa
672 Fluor 488-conjugated goat anti-mouse IgG (Thermo Fisher Scientific) as
673 described previously (36).

674 **Fusion assay**

675 The fusion activity for modified GP64 proteins was measured as previously
676 described (36). Briefly, Sf9 cells in 12-well plates were transfected with
677 plasmids (2 μg DNA for each plasmid expressing the modified GP64 or
678 0.005-2 μg DNA for the plasmid expressing WT GP64) or infected with the
679 virus encoding WT or the modified GP64 (MOI=5). At 36 h p.t. or 48 h p.i., the
680 cells were incubated in PBS at pH 5.0 for 3 min. After washing once with PBS
681 at pH 7.4, the cells were maintained in TNMFH medium at 27 °C for 4 h. Then,
682 the transfected or infected cells were fixed with methanol and stained with 0.1%
683 Eosin Y and 0.1% methylene blue. The number of nuclei found in syncytia that
684 containing at least five nuclei was scored. The ratio of nuclei in syncytial
685 masses to those in a field were calculated and then normalized to those from
686 WT GP64 that was localized to the cell surface at equivalent levels.

687 **Hemifusion and pore formation assay**

688 The hemifusion and pore formation assay was performed as previously

described with minor modifications (36). Briefly, rabbit red blood cells (RBCs) were collected by centrifugation of the fresh blood at 500 *g*, 4°C for 5 min. After washing twice with PBS (pH 7.4), the cells were dual-labeled with R18 and calcein-AM (Invitrogen). At 36 h p.t. or 48 h p.i., the transfected or infected Sf9 cells were washed twice with PBS (pH 7.4) and then incubated with the labeled RBCs for 20 min. After removing the unbound RBCs, the cells were washed three times with PBS (pH 7.4). Then, the cells were incubated in PBS at pH 5.0 for 3 min. After washing twice with PBS (pH 7.4), the cells were maintained in TNMFH medium at 27 °C for 20 min. Then, the transfer of fluorescence between RBCs and Sf9 cells was photographed using epifluorescence microscopy (Nikon Eclipse Ti). Five fields were randomly selected to score for dye transfer. The efficiency of hemifusion or pore formation was estimated by the ratio of R18-transferred Sf9 cells or calcein-AM-transferred Sf9 cells to RBC-bound Sf9 cells.

Transfection-infection assay

Sf9 cells in 6-well plates were transfected with 4 μg of each of the recombinant AcMNPV bacmids encoding WT or the modified GP64. At 96 h p.t. the supernatants were collected and clarified by centrifugation (3,000 *g*, 10 min), and then used to infect a new monolayer of Sf9 cells. At 96 h p.i. the supernatants were harvested and the infectious virus titers were determined by a 50% tissue culture infection dose ($TCID_{50}$) assay.

Virus growth curve analysis

Sf9 cells in 12-well plates were infected with the virus expressing WT or the modified GP64 at an MOI of 5 or 0.1 for 1 h. After removing the viral inoculum, the cells were washed once with TNMFH medium and then incubated at 27 °C.

714 At different time points (24-120 h) p.i., the cell culture supernatant was
715 collected and infectious virus titers were determined by $TCID_{50}$ assays.

716 **BVs purification**

717 BVs were purified as previously described with minor modifications (41).
718 Briefly, Sf9 cells were infected with the virus expressing WT or the modified
719 GP64 (E390A, G391A, or N381/K389A) with an MOI of 1. At 96 h p.i.,
720 infected-cell supernatants were centrifuged at 28000 rpm, 4°C for 90 min
721 through a 25% (wt/vol) sucrose cushion. Pellets were resuspended and
722 overlaid onto a 30-55% (wt/vol) continuous sucrose gradient and centrifuged at
723 28000 rpm, 4°C for 90 min. Then, the virus fraction was diluted with TNMFH
724 medium, and centrifuged again under the same condition. Virus pellets were
725 resuspended in TNMFH medium and the potential contamination was removed
726 by filtration. Virus titers were determined by $TCID_{50}$ assays.

727 **BVs binding and internalization assay**

728 Sf9 cells in 12-well plates were pre-chilled at 4 °C for 30 min and then
729 incubated with the purified virus expressing WT or the modified GP64 (E390A,
730 G391A, or N381/K389A) (MOI=5) at 4°C for 1 h. After removing the virus
731 inoculum, cells were washed twice with cold TNMFH medium. Then, one set of
732 the cells were collected and total DNA was extracted at 4 °C by using DNeasy
733 Blood & Tissue kit (QIAGEN). Another set of the cells was incubated at 27 °C
734 for 1 h to allow virus internalization. Then, the cells were treated with citrate
735 buffer (40 mM sodium citrate, 135 mM NaCl, and 10 mM KCl, pH 3.1) for 1 min
736 to inactivate and remove non-internalized viruses as described previously (15)
737 and then total DNA was extracted. Viral genomic DNA in total DNA extracts
738 that isolated from two sets of the infected cells was measured by qPCR

(CFX96 Touch™ real-time PCR system, Bio-Rad). Each PCR mixture contained 10 µl SYBR® Premix ExTaq II (TaKaRa), 2.5 µM each primer (ODV-e56F: 5'-GATCTTCCTGCGGGCCAAACACT-3' and ODV-e56R: 5'-AACAAGACCGCGCCTATCAACAAA-3'), and 1 ng of the DNA. A standard curve was generated by using the plasmid ODV-e56pGEM as previously described (42).

Virus egress assay

Sf9 cells in 6-well plates were transfected with 4 µg of each of the recombinant AcMNPV bacmids which express the modified GP64 (E390A, G391A, or N381/K389A) or 0.5-4 µg of the bacmid expressing WT GP64. At 24 h p.t., one set of the cells were used to score GFP fluorescence-positive cells under an epifluorescence microscope and evaluate the transfection efficiency. Another set of the cells were solubilized with 0.5% NP-40 in PBS (pH 7.4) and the β-Gluc activity was measured using the substrate 4-Nitrophenyl β-D-glucuronide (PNPG, Sigma-Aldrich). The cell supernatants in third set of the transfected cells were collected and infectious virus titers were determined by $TCID_{50}$ assays, the cells were fixed with 0.5% glutaradehyde and cell surface levels of GP64s were assessed by cELISA with the MAb AcV5.

Western blotting

Transfected or infected Sf9 cells were lysed with Triton X-100 buffer (150 mM sodium chloride, 0.1% Triton X-100, 50 mM Tris, pH 8.0) containing the protease inhibitor cocktail (Roche Life Science). The extracted proteins were separated by 6% or 10% SDS-polyacrylamide gels under reducing and non-reducing conditions. After transferring to a PVDF membrane (Millipore), the blots were blocked in a 4% milk TBST (10 mM Tris pH 8.0, 150 mM sodium

chloride, 0.05% Tween-20) solution. GP64 proteins were detected with the MAb AcV5 and the alkaline phosphatase-conjugated goat anti-mouse IgG (Promega). Immunoblots were visualized using Nitro-Blue-Tetrazolium (NBT) and 5-Bromo-4-Chloro-3-Indolyl Phosphate (BCIP) (Promega).

Acknowledgements

We thank Yuying Li for technical assistance. This work was supported by grants from National Key R&D Program of China (2017YFC1200605) and National Natural Science Foundation of China (NSFC, No. 31672082).

Reference

1. **Plemper RK.** 2011. Cell entry of enveloped viruses. Curr Opin Virol **1:**92-100.
2. **Li Y, Modis Y.** 2014. A novel membrane fusion protein family in Flaviviridae? Trends Microbiol **22:**176-182.
3. **White JM, Delos SE, Brecher M, Schornberg K.** 2008. Structures and mechanisms of viral membrane fusion proteins: multiple variations on a common theme. Crit Rev Biochem Mol Biol **43:**189-219.
4. **Podbilewicz B.** 2014. Virus and cell fusion mechanisms. Annu Rev Cell Dev Biol **30:**111-139.
5. **Rohrmann G.** 2019. Baculovirus Molecular Biology: Fourth Edition [Internet]. National Center for Biotechnology Information (US), Bethesda (MD).
6. **Harrison RL, Herniou EA, Jehle JA, Theilmann DA, Burand JP, Becnel JJ, Krell PJ, van Oers MM, Mowery JD, Bauchan GR, Ictv Report C.** 2018. ICTV virus taxonomy profile: Baculoviridae. J Gen Virol **99:**1185-1186.
7. **van Oers MM, Pijlman GP, Vlak JM.** 2015. Thirty years of baculovirus-insect cell protein expression: from dark horse to mainstream technology. J Gen Virol **96:**6-23.
8. **Tsai CH, Wei SC, Lo HR, Chao YC.** 2020. Baculovirus as versatile vectors for protein display and biotechnological applications. Curr Issues Mol Biol **34:**231-256.
9. **Blissard GW, Theilmann DA.** 2018. Baculovirus entry and egress from insect cells. Annu Rev Virol **5:**113-139.
10. **Wang X, Liu X, Makalliwa GA, Li J, Wang H, Hu Z, Wang M.** 2017. Per os infectivity factors: a complicated and evolutionarily conserved entry machinery of baculovirus. Sci China. Life Sci **60:**806-815.
11. **Hefferon KL, Oomens AG, Monsma SA, Finnerty CM, Blissard GW.** 1999. Host cell receptor binding by baculovirus GP64 and kinetics of virion entry. Virology **258:**455-468.
12. **Zhou J, Blissard GW.** 2008. Identification of a GP64 subdomain involved in receptor binding by budded virions of the baculovirus Autographica californica multicapsid nucleopolyhedrovirus. J Virol **82:**4449-4460.
13. **Monsma SA, Oomens AG, Blissard GW.** 1996. The GP64 envelope fusion protein is an essential baculovirus protein required for cell-to-cell transmission of infection. J Virol

70:4607-4616.

14. **Long G, Pan X, Kormelink R, Vlak JM.** 2006. Functional entry of baculovirus into insect and mammalian cells is dependent on clathrin-mediated endocytosis. J Virol **80:**8830-8833.
15. **Yue Q, Li J, Guo Y, Yan F, Liu X, Blissard GW, Li Z.** 2020. Efficient entry of budded virions of Autographa californica multiple nucleopolyhedrovirus into Spodoptera frugiperda cells is dependent on dynamin, Rab5, and Rab11. Insect Biochem Mol Biol **123:**103409.
16. **Blissard GW, Wenz JR.** 1992. Baculovirus gp64 envelope glycoprotein is sufficient to mediate pH-dependent membrane fusion. J Virol **66:**6829-6835.
17. **Li Z, Blissard GW.** 2011. Autographa californica multiple nucleopolyhedrovirus GP64 protein: roles of histidine residues in triggering membrane fusion and fusion pore expansion. J Virol **85:**12492-12504.
18. **Kadlec J, Loureiro S, Abrescia NG, Stuart DI, Jones IM.** 2008. The postfusion structure of baculovirus gp64 supports a unified view of viral fusion machines. Nat Struct Mol Biol **15:**1024-1030.
19. **Oomens AG, Blissard GW.** 1999. Requirement for GP64 to drive efficient budding of Autographa californica multicapsid nucleopolyhedrovirus. Virology **254:**297-314.
20. **Wang Q, Bosch BJ, Vlak JM, van Oers MM, Rottier PJ, van Lent JWM.** 2016. Budded baculovirus particle structure revisited. J Invertebr Pathol **134:**15-22.
21. **Li Z, Blissard GW.** 2010. Baculovirus GP64 disulfide bonds: the intermolecular disulfide bond of Autographa californica multicapsid nucleopolyhedrovirus GP64 is not essential for membrane fusion and virion budding. J Virol **84:**8584-8595.
22. **Backovic M, Jardetzky TS.** 2011. Class III viral membrane fusion proteins. Adv Exp Med Biol **714:**91-101.
23. **Peng R, Zhang S, Cui Y, Shi Y, Gao GF, Qi J.** 2017. Structures of human-infecting Thogotovirus fusogens support a common ancestor with insect baculovirus. Proc Natl Acad Sci USA **114:**E8905-E8912.
24. **Roche S, Bressanelli S, Rey FA, Gaudin Y.** 2006. Crystal structure of the low-pH form of the vesicular stomatitis virus glycoprotein G. Science **313:**187-191.
25. **Roche S, Rey FA, Gaudin Y, Bressanelli S.** 2007. Structure of the prefusion form of the vesicular stomatitis virus glycoprotein G. Science **315:**843-848.
26. **Baquero E, Albertini AA, Gaudin Y.** 2015. Recent mechanistic and structural insights on class III viral fusion glycoproteins. Curr Opin Struct Biol **33:**52-60.
27. **Kim IS, Jenni S, Stanifer ML, Roth E, Whelan SP, van Oijen AM, Harrison SC.** 2017. Mechanism of membrane fusion induced by vesicular stomatitis virus G protein. Proc Natl Acad Sci USA **114:**E28-E36.
28. **Dong S, Blissard GW.** 2012. Functional analysis of the Autographa californica multiple nucleopolyhedrovirus GP64 terminal fusion loops and interactions with membranes. J Virol **86:**9617-9628.
29. **Backovic M, Longnecker R, Jardetzky TS.** 2009. Structure of a trimeric variant of the Epstein-Barr virus glycoprotein B. Proc Natl Acad Sci USA **106:**2880-2885.
30. **Heldwein EE, Lou H, Bender FC, Cohen GH, Eisenberg RJ, Harrison SC.** 2006. Crystal structure of glycoprotein B from herpes simplex virus 1. Science **313:**217-220.
31. **Bai C, Qi J, Wu Y, Wang X, Gao GF, Peng R, Gao F.** 2019. Postfusion structure of human-infecting Bourbon virus envelope glycoprotein. J Struct Biol **208:**99-106.

32. **Si Z, Zhang J, Shivakoti S, Atanasov I, Tao CL, Hui WH, Zhou K, Yu X, Li W, Luo M, Bi GQ, Zhou ZH.** 2018. Different functional states of fusion protein gB revealed on human cytomegalovirus by cryo electron tomography with Volta phase plate. PLoS Pathog **14:**e1007452.
33. **Zhang Y.** 2008. I-TASSER server for protein 3D structure prediction. BMC Bioinformatics **9:**40.
34. **Jarvis DL, Wills L, Burow G, Bohlmeyer DA.** 1998. Mutational analysis of the N-linked glycans on Autographa californica nucleopolyhedrovirus gp64. J Virol **72:**9459-9469.
35. **Zhou J, Blissard GW.** 2006. Mapping the conformational epitope of a neutralizing antibody (AcV1) directed against the AcMNPV GP64 protein. Virology **352:**427-437.
36. **Li Z, Blissard GW.** 2008. Functional analysis of the transmembrane (TM) domain of the Autographa californica multicapsid nucleopolyhedrovirus GP64 protein: substitution of heterologous TM domains. J Virol **82:**3329-3341.
37. **Hohmann AW, Faulkner P.** 1983. Monoclonal antibodies to baculovirus structural proteins: determination of specificities by Western blot analysis. Virology **125:**432-444.
38. **Connolly SA, Longnecker R.** 2012. Residues within the C-terminal arm of the herpes simplex virus 1 glycoprotein B ectodomain contribute to its refolding during the fusion step of virus entry. J Virol **86:**6386-6393.
39. **Hussein HA, Walker LR, Abdel-Raouf UM, Desouky SA, Montasser AK, Akula SM.** 2015. Beyond RGD: virus interactions with integrins. Arch Virol **160:**2669-2681.
40. **Burke HG, Heldwein EE.** 2015. Crystal structure of the human cytomegalovirus glycoprotein B. PLoS Pathog **11:**e1005227.
41. **Guo Y, Yue Q, Gao J, Wang Z, Chen YR, Blissard GW, Liu TX, Li Z.** 2017. Roles of cellular NSF protein in entry and nuclear egress of budded virions of Autographa californica multiple nucleopolyhedrovirus. J Virol **91**. doi: 10.1128/JVI.01111-17.
42. **Li Z, Blissard GW.** 2012. Cellular VPS4 is required for efficient entry and egress of budded virions of Autographa californica multiple nucleopolyhedrovirus. J Virol **86:**459-472.
43. **Luckow VA, Lee SC, Barry GF, Olins PO.** 1993. Efficient generation of infectious recombinant baculoviruses by site-specific transposon-mediated insertion of foreign genes into a baculovirus genome propagated in Escherichia coli. J Virol **67:**4566-4579.

876 **Figure legends**

877 **Figure 1**

878 **The conformation and amino acid contacts of domain IV of AcMNPV**
879 **GP64**. (A, B) Postfusion structure of GP64 monomer and trimer (PDB, ID:
880 3DUZ) (18). Domains I-V (DI-DV) in the monomer are colored as green, red,
881 blue, cyan, and magenta, respectively. The conformation of residues
882 V394-D398 in domain IV that has not been solved in the structure is predicted
883 and showed in gray. L1, loop1; L2, loop2; FL1, fusion loop1; FL2, fusion loop2.
884 (C) Domain IV and a portion of domain III are shown both in ribbon and surface
885 representation. The conserved amino acids in domain IV among baculovirus
886 GP64s and thogotovirus glycoproteins are displayed in sticks. The cluster of
887 E390-G391-R392 and the disulfide bond C382-C402 are shown as spheres.
888 (D) The contacts in domain IV of GP64. (E) Amino acid sequence alignments
889 of domain IV of baculovirus GP64s and thogotoviruses glycoproteins. A
890 schematic diagram of AcMNPV GP64 is shown at the top of the alignment. SP,
891 signal peptide; PTM, pre-transmembrane domain; TM, transmembrane
892 domain. The color code for each domain (DI-IV) is the same as in (A). Two
893 epitopes in domain III and domain V that separately recognized by the MAb
894 AcV1 and AcV5 are shown. Virus name abbreviations are listed as that on the
895 ICTV website (https://talk.ictvonline.org/).

896 **Figure 2**

897 **Expression and cell surface localization of the modified GP64**. (A)
898 Western blotting analysis of expression and trimerization of WT and modified
899 GP64 proteins on non-reducing (NR) and reducing (R) gels. Sf9 cells were
900 transfected with the plasmid expressing each of the WT or modified GP64s. At

36 h p.t., the expression of GP64 was detected. (B) Relative cell surface levels of GP64 were determined by cELISA. A standard curve generated by transfecting Sf9 cells with decreasing quantities of the plasmid expressing WT GP64 is shown on the left side of the panel. Cells were transfected with 2 μg of the plasmid expressing each modified GP64. Error bars represent standard deviations (SD) from the mean of three replicates. (C) A diagram of domain IV shows the contacts and residues identified as critical for cell surface localization of GP64. L1, loop1; L2, loop2.

Figure 3

Cell-cell fusion mediated by WT and the modified GP64. (A) Cell-cell syncytium formation assay. Sf9 cells were transfected with the plasmid expressing WT or the modified GP64. At 36 h p.t., the syncytium formation was induced by the low-pH treatment and photographed using phase-contrast microscopy. Arrows indicate syncytial masses. (B) Analysis of relative fusion activity for each construct. Error bars represent SD from the mean of three replicates. (C) A diagram of domain IV shows the contacts and residues identified as critical for membrane fusion. L1, loop1; L2, loop2.

Figure 4

Hemifusion and pore formation mediated by fusion-deficient GP64 proteins. (A) A schematic of hemifusion and pore formation assay. Sf9 cells were transfected with the plasmid expressing WT or the modified GP64. At 36 h p.t., the cells were incubated with dual dye (R18 and calcein-AM)-labeled RBCs. After removing the unattached RBCs, the cells were treated with PBS (pH 5.0) for 3 min to induce fusion. Transfer of R18 between RBCs and Sf9 cells indicates the merger of outer membrane leaflets of two kinds of cells

(hemifusion), whereas the transfer of calcein-AM between RBCs and Sf9 suggests the inner membrane leaflets merger of the cells (pore formation). (B) Hemifusion and pore formation assay. Sf9 cells were transfected with 2 μg or 0.005 μg plasmid expressing WT GP64 (WT2 or WT0.005) or with 2 μg of the plasmid expressing each mutated GP64. At 36 h p.t., Sf9 cells were incubated with dual dye-labeled RBCs and the dye transfer between RBCs and Sf9 cells were observed and photographed. The dye transfer efficiency was estimated by the ratio of the number of R18-transferred or calcein-AM-transferred Sf9 cells to the number of Sf9 cells with RBCs bound (C). Error bars represent SD from the mean of three replicates.

Figure 5

Analysis of low-pH triggered conformational change of the fusion-deficient GP64 constructs. The conformational change of cell-surface localized GP64 proteins upon low-pH trigger was measured by cELISA using the MAb AcV1. Sf9 cells were transfected with 2 μg of the plasmid for WT or each modified GP64. Each value represents the mean from triplicate transfections and is normalized to that of Sf9 cells transfected with the plasmid expressing WT GP64 at pH 7.0.

Figure 6

Growth kinetics of viruses expressing fusion-deficient GP64 constructs. Sf9 cells were infected with the virus expressing WT or each modified GP64 at an MOI of 5 (A, B, left panels) or at an MOI of 0.1 (A, B, right panels). At the indicated time points p.i., virus titers were determined by $TCID_{50}$ assays. Error bars represent SD from the mean of three replicates.

Figure 7

951 **Effects of E390A, G391A, and N381/K389A on membrane fusion and**
952 **conformational change of the modified GP64 in virus-infected cells**. Sf9
953 cells were infected with the virus expressing either WT GP64 or E390A,
954 G391A, or N381/K389A (MOI=5). At 48 h p.i., the cells were subjected to
955 analysis. (A) Western blot analysis of the expression of GP64 proteins under
956 non-reducing (NR) and reducing (R) conditions. (B) Relative cell surface levels
957 of GP64 proteins were determined by cELISA. (C, D) Cell-cell fusion assay.
958 The infected cells were incubated with PBS (pH 5.0) for 3 min and then
959 cultured at 27 °C for 4 h. Then, the syncytium formation was observed and
960 photographed (C) and the percentage of cells in syncytial masses (≥5 nuclei)
961 was calculated (D). (E, F) Hemifusion and pore formation assay. The infected
962 cells were incubated with dual dye-labeled RBCs. After attachment, the cells
963 were incubated with PBS (pH 5.0) and then the dye transfer between RBCs
964 and Sf9 cells were observed and photographed (E) and the dye transfer
965 efficiency was estimated as described above (F). (G) Low-pH triggered
966 conformational change of WT and the modified GP64. The infected cells were
967 incubated in PBS with varying pH values (pH 4.5-7.0) and then fixed and
968 analyzed by cELISA using the MAb AcV1. Error bars represent SD from the
969 mean of three replicates.

970 **Figure 8**

971 **Effects of E390A, G391A, and N381/K389A on BVs binding and**
972 **internalization (A) and infectious BVs egress (B).** (A) (a) Schematic
973 representation of BVs binding and internalization assays. Sf9 cells were
974 incubated with each of the virus expressing WT GP64 or E390A, G391A, or
975 N381/K389A (MOI=5) at 4°C. After removing the virus inoculum and washing

976 the cells, one set of the cells was lysed and virus binding efficiency was
977 determined by measuring viral genomic DNA using qPCR (b). The other set of
978 cells was cultured at 27 °C for 1 h and then the virus internalization was
979 examined by qPCR of viral genomic DNA (c). (B) (a) Schematic representation
980 of BVs egress assay. Sf9 cells were transfected with 0.5-4 μg bacmid DNA
981 expressing WT GP64 or with 4 μg bacmid DNA expressing either E390A,
982 G391A, or N381/K389A. At 24 h p.t., the relative cell surface levels of GP64
983 proteins were determined by cELISA (b) and infectious virus production was
984 measured by $TCID_{50}$ assays (c). Error bars represent SD from the mean of
985 three replicates. ***, $P<0.0005$ (by paired two-tailed *t* test).

986 **Figure 9**

987 **Proposed roles of domain IV in membrane fusion and low-pH triggered**
988 **conformational change of AcMNPV GP64.** (A) The predicted prefusion
989 structure of AcMNPV GP64 (domain I-IV) that was generated by I-TASSER
990 approach using the prefusion structure of VSV G (PDB, ID: 5i2s) (25) as the
991 template (left panel), the postfusion structure of GP64 (middle panel), and the
992 critical residues and contacts within domain IV that are involved in GP64
993 conformation change and membrane fusion (right panel). Domains I-V (DI-DV),
994 PTM (pre-transmembrane domain), and TM (transmembrane domain) are
995 colored in green, red, blue, cyan, magenta, orange, and olive, respectively.
996 FL1, fusion loop1; FL2, fusion loop2. Residues and the contacts are indicated
997 as magenta spheres and sticks, respectively. (B) Roles of domain IV in
998 prefusion to postfusion conformation change of GP64. In prefusion state
999 (neutral-pH conditions), GP64 is anchored on the viral envelope (or the cell
1000 surface) in a compact form. Upon low-pH trigger, the structure of GP64 opens

1001 to expose fusion loops that reside at the tip of domain I (step 1). Following the
1002 extension of domain V and the formation of long α-helix in domain III, fusion
1003 loops target the cellular membrane and interact with it (step 2). Refolding of
1004 GP64 that may drive by the formation of long coiled-coils in the center of
1005 domain III and the interaction of domain III, IV, and V promotes the close of two
1006 membranes in proximal and yields the outer membrane leaflets merger
1007 (hemifusion, step 3a) and the inner membrane leaflets merger (fusion pore
1008 formation and expansion, step 3b). The potential negative effects of mutations
1009 in domain IV on membrane fusion and conformational change of GP64 are
1010 indicated.

Figure 1

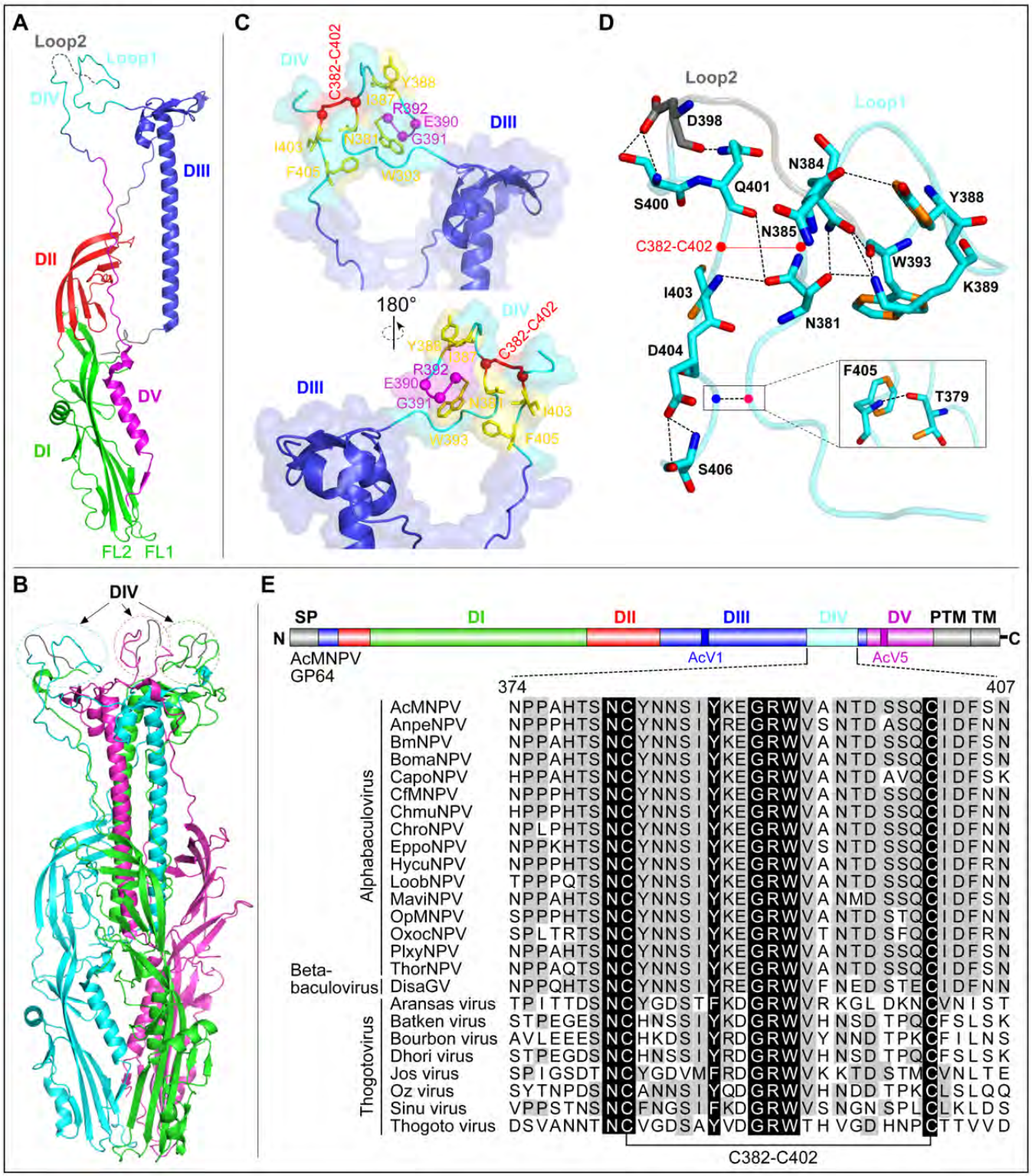

Figure 2

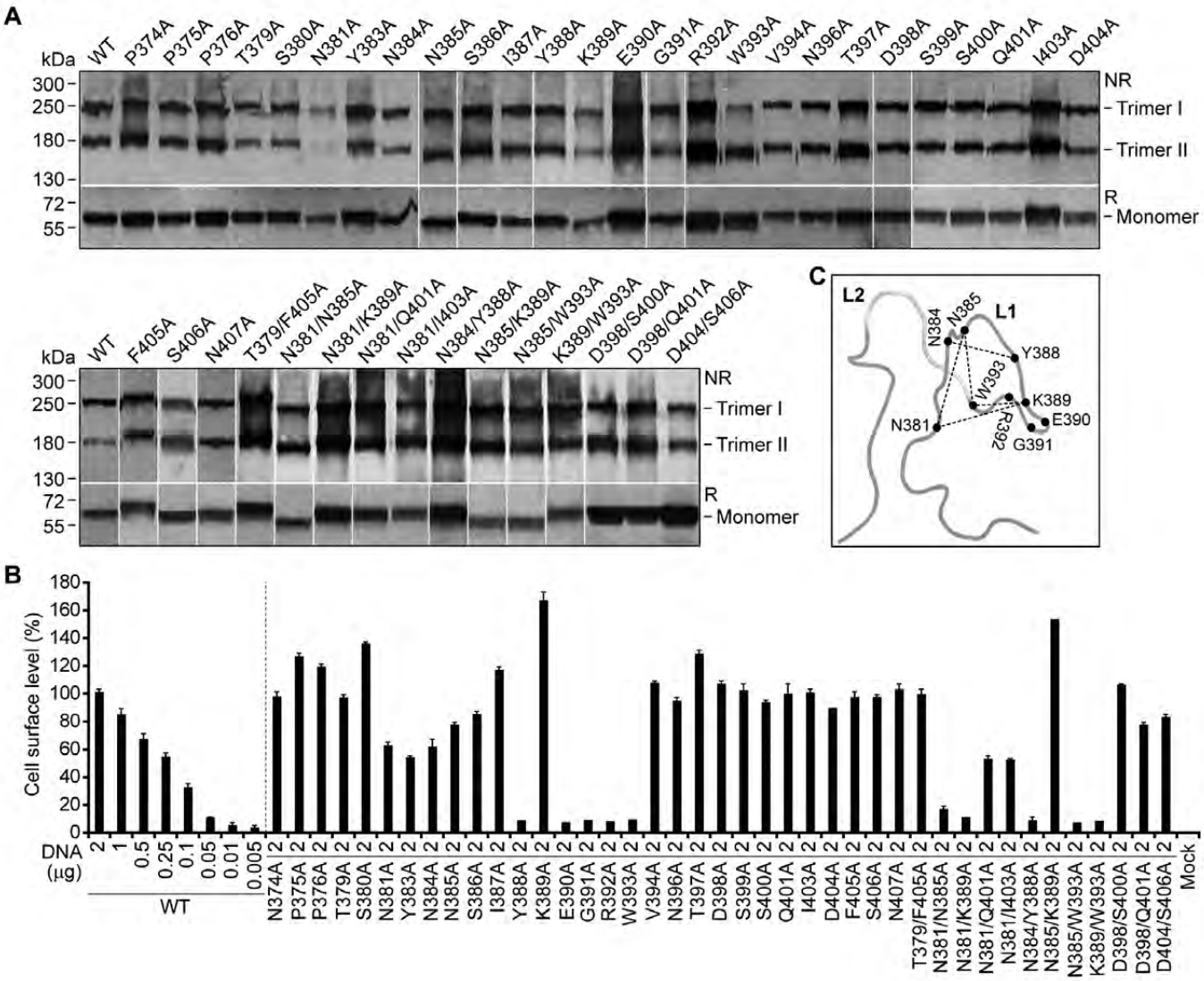

Figure 3

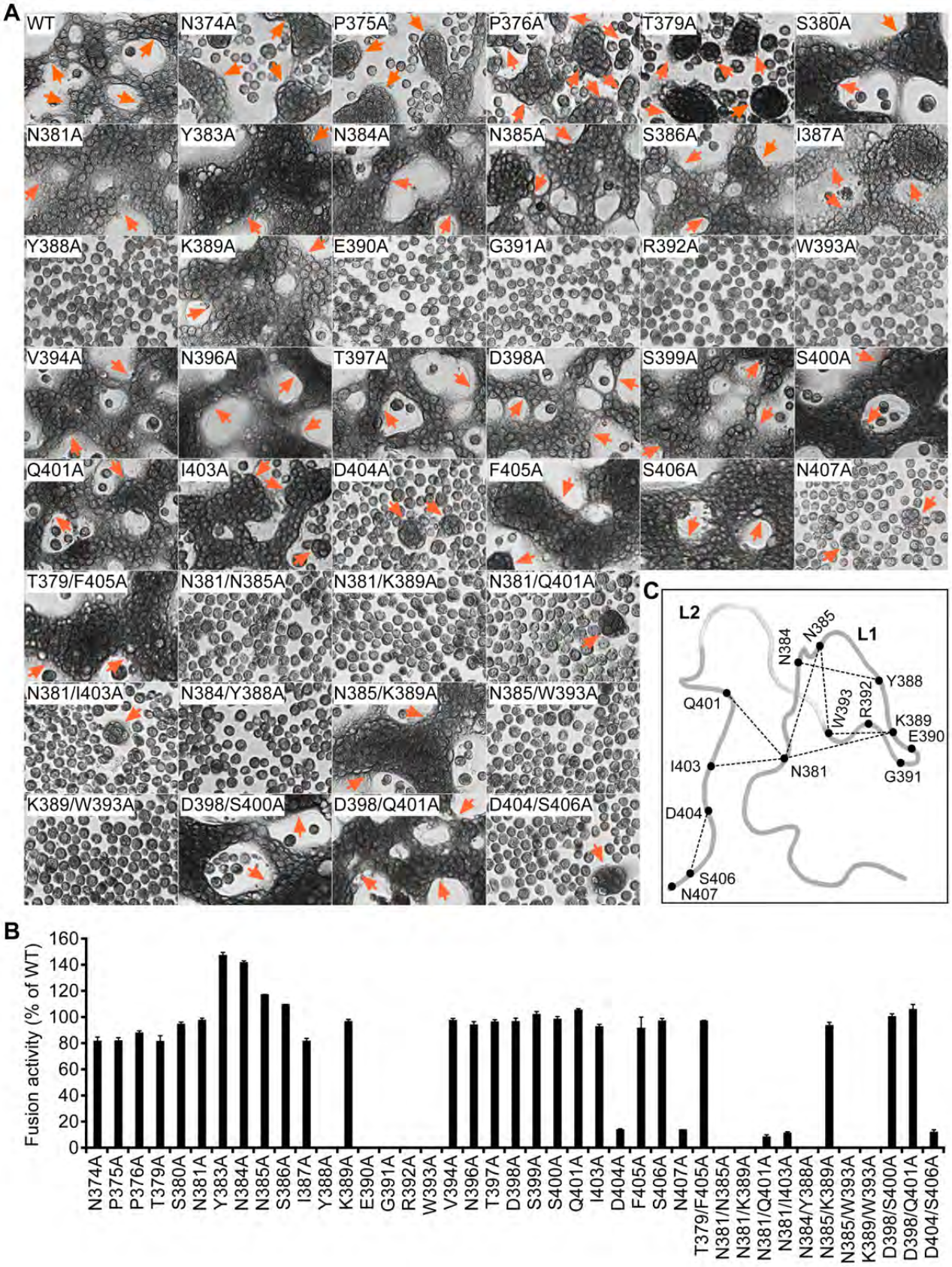

Figure 4

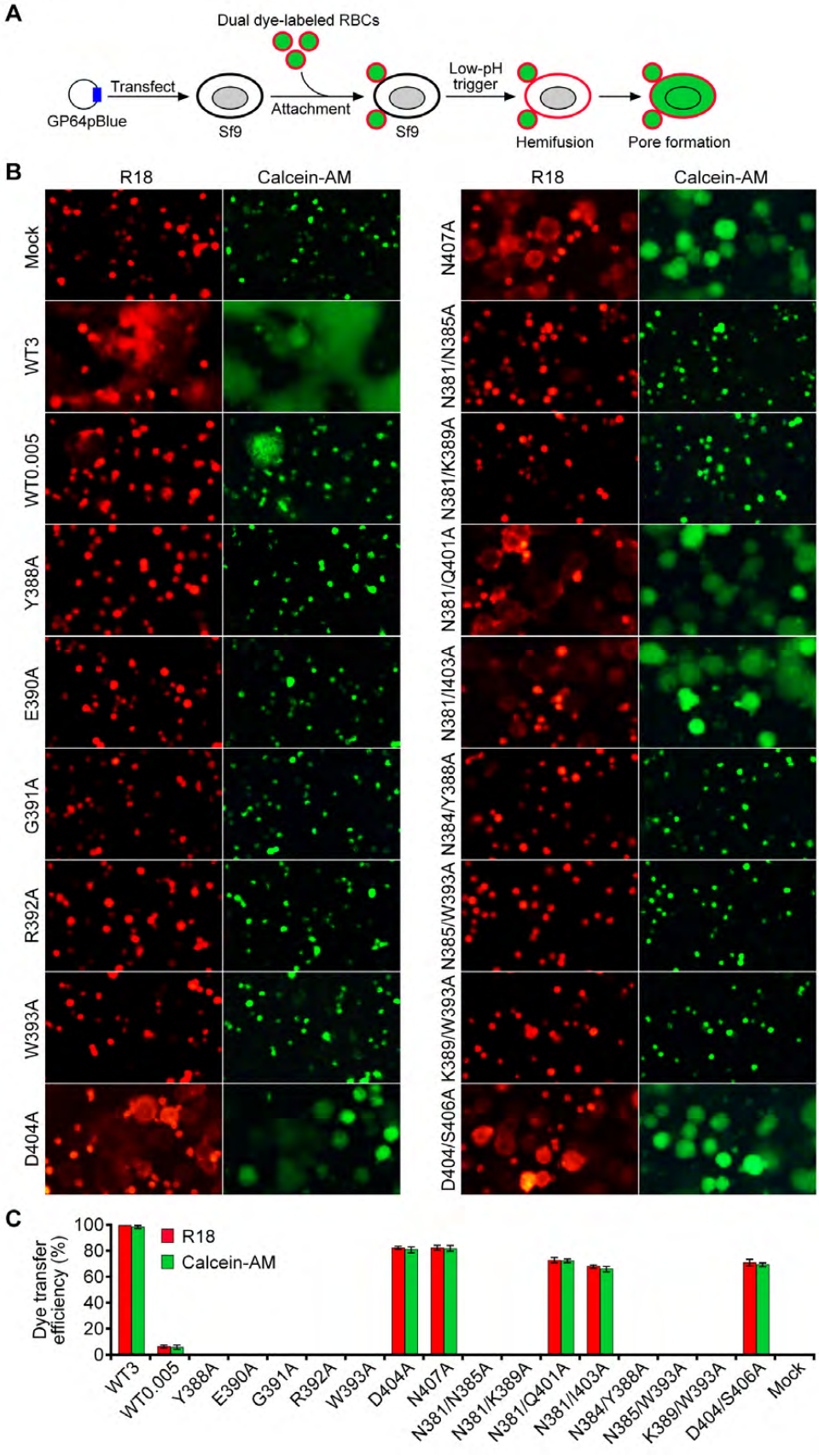

Figure 5

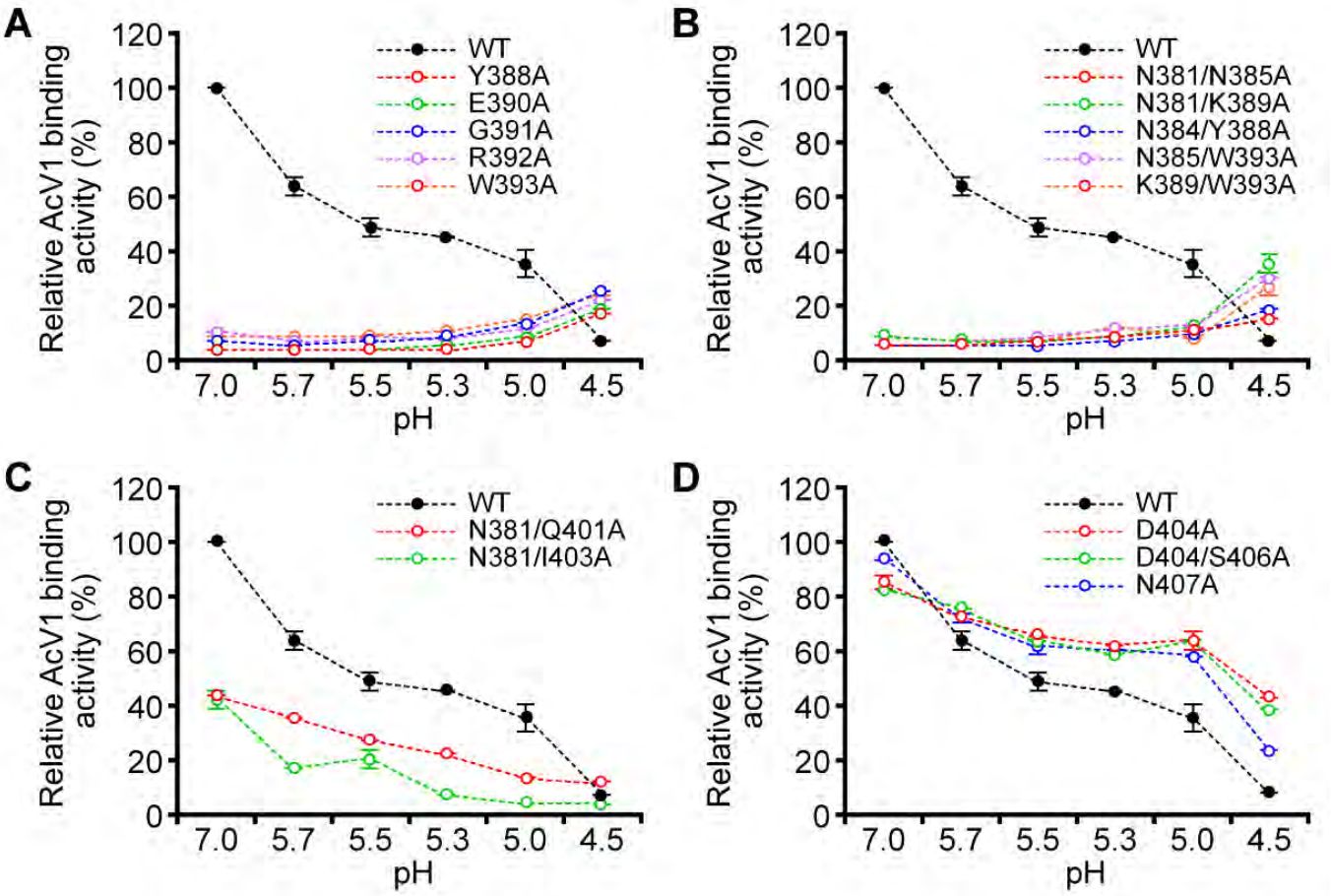

Figure 6

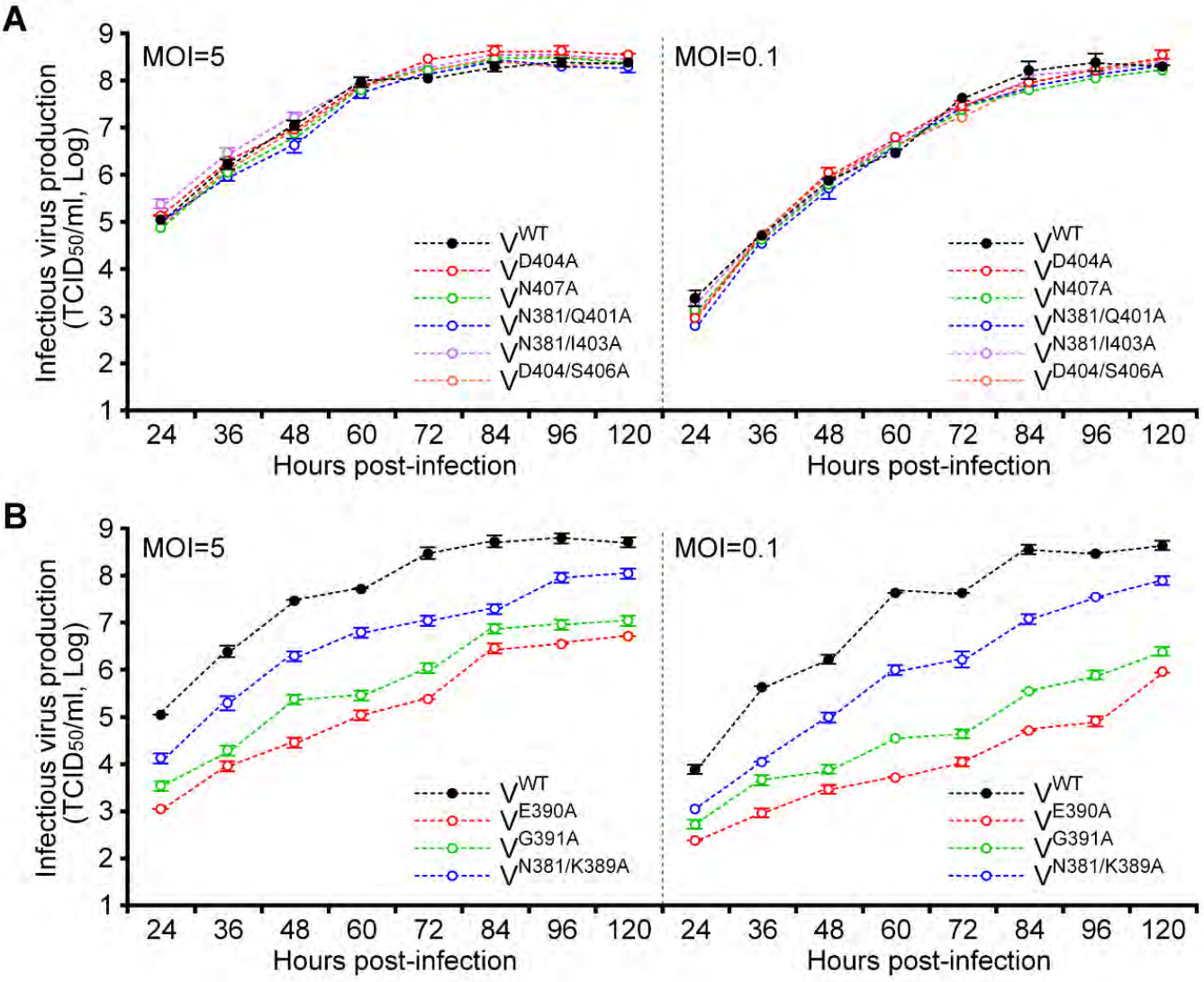

Figure 7

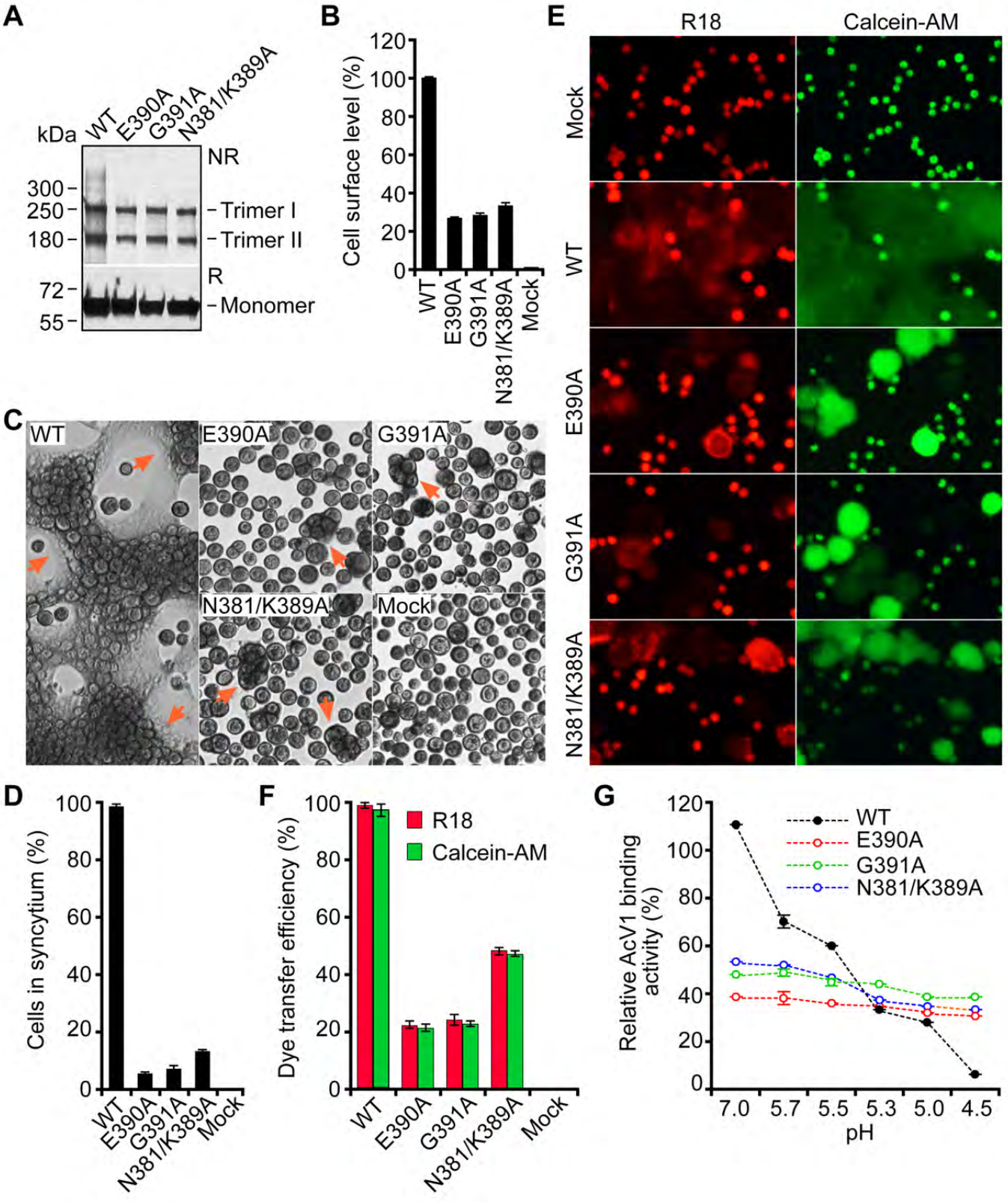

Figure 8

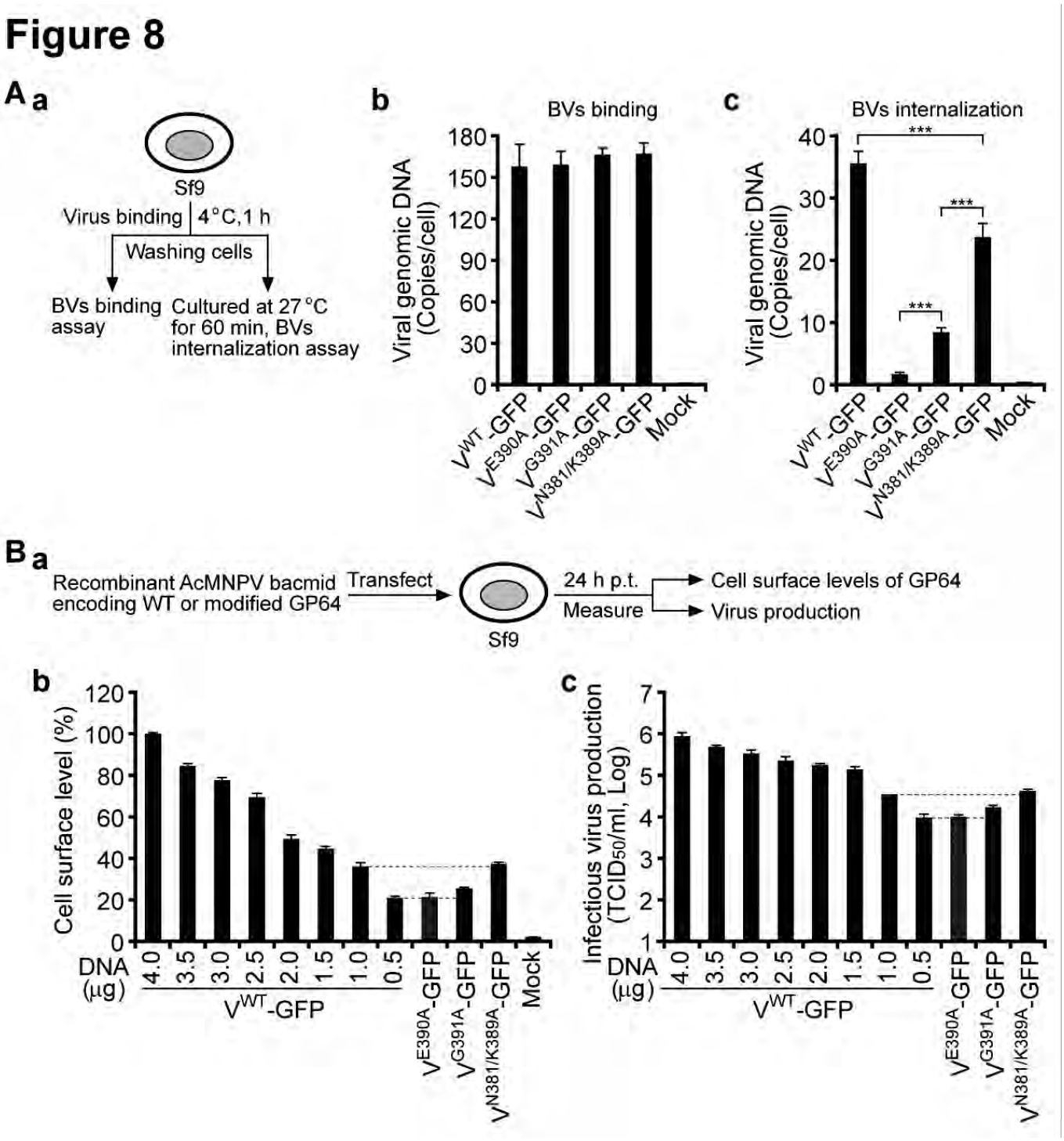

Figure 9

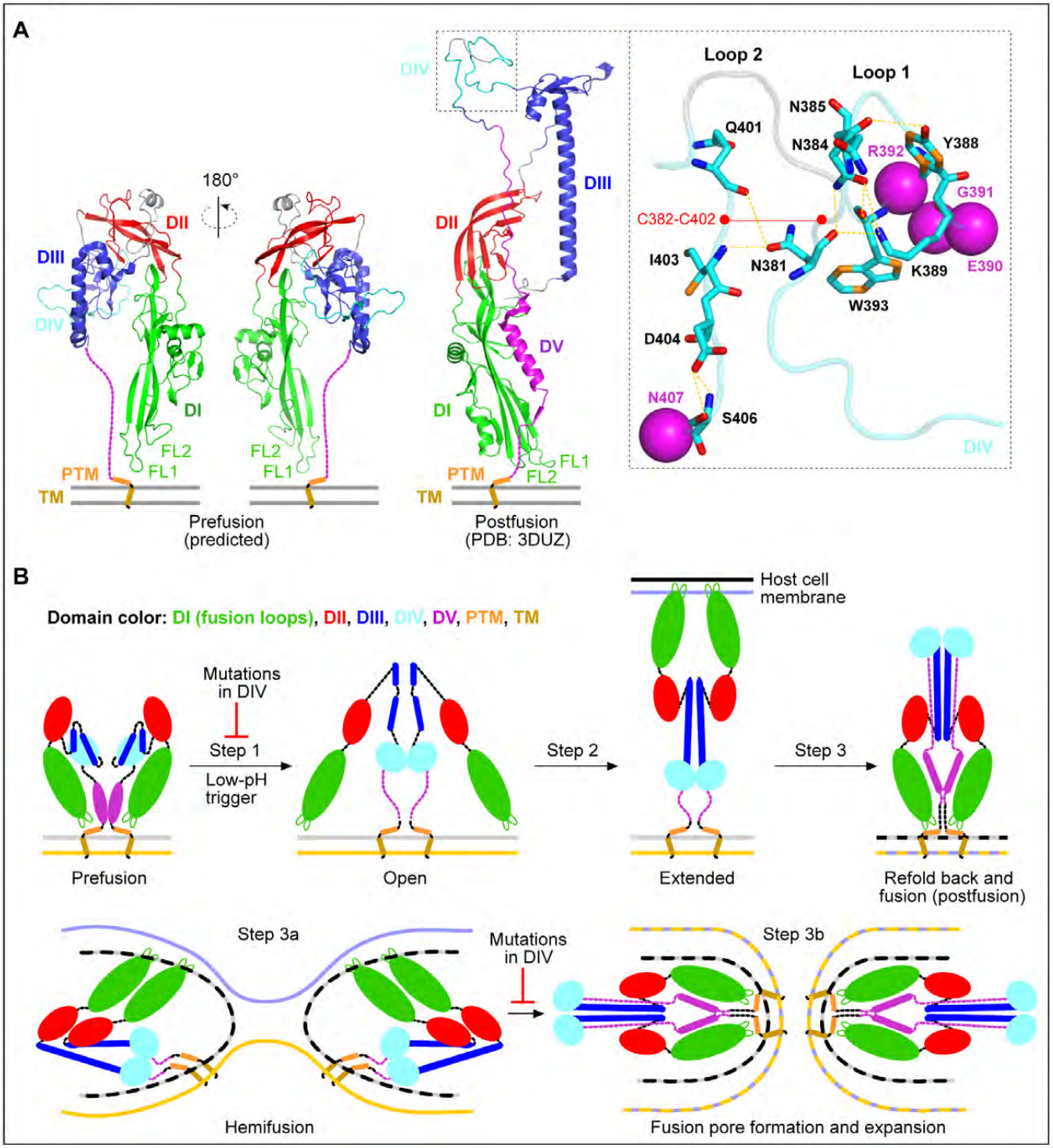

Table 1. Phenotypes of wild-type and alanine-substitutions in domain IV of AcMNPV GP64

Construct	Contacts[a]	Trimer	Surface (%)	Fusion (%)	Dye transfer (%)		Virus infectivity[b]	
					R18	Calcein-AM	Rescue	Virus titer ($TCID_{50}$/ml)
WT	√	+	100.0±2.9	97.9±1.3	99.5±0.3	99.2±0.3	+	$(2.4±0.3)×10^8$
N374A	-	+	97.3±2.7	81.0±2.0	ND	ND	+	$(1.8±0.0)×10^8$
P375A	-	+	127.4±1.3	81.8±1.6	ND	ND	+	$(1.5±0.0)×10^8$
P376A	-	+	118.4±1.1	87.9±1.5	ND	ND	+	$(2.2±0.6)×10^8$
T379A	√	+	96.8±3.0	81.1±3.5	ND	ND	+	$(1.1±0.1)×10^8$
S380A	-	+	135.4±1.8	95.0±0.7	ND	ND	+	$(1.9±0.5)×10^8$
N381A	√	+	62.0±2.9	97.7±1.3	ND	ND	+	$(2.2±0.1)×10^8$
Y383A	-	+	53.3±1.6	147.2±2.3	ND	ND	+	$(1.0±0.2)×10^8$
N384A	√	+	60.8±5.7	141.6±1.6	ND	ND	+	$(2.0±0.3)×10^8$
N385A	√	+	76.3±2.2	117.1±0.2	ND	ND	+	$(2.4±0.3)×10^8$
S386A	-	+	85.1±1.3	108.8±0.8	ND	ND	+	$(1.7±0.2)×10^8$
I387A	-	+	116.8±2.0	81.7±1.6	ND	ND	+	$(1.7±0.2)×10^8$
Y388A	×	+	6.5±0.2	0	0	0	-	NA
K389A	√	+	166.6±6.8	97.1±0.4	ND	ND	+	$(1.5±0.4)×10^8$
E390A	-	+	6.1±0.5	0	0	0	+	$(1.4±0.2)×10^6$
G391A	-	+	6.7±0.3	0	0	0	+	$(2.2±0.0)×10^6$
R392A	-	+	6.0±0.3	0	0	0	-	NA
W393A	×	+	7.3±0.2	0	0	0	-	NA
V394A	-	+	107.5±0.8	96.9±1.4	ND	ND	+	$(1.1±0.1)×10^8$
N396A	-	+	94.0±3.1	93.4±2.5	ND	ND	+	$(1.4±0.2)×10^8$
T397A	-	+	128.9±2.4	96.2±1.3	ND	ND	+	$(5.1±0.7)×10^8$
D398A	×	+	106.4±2.8	96.8±1.1	ND	ND	+	$(4.2±0.6)×10^8$
S399A	-	+	101.4±5.0	101.6±1.6	ND	ND	+	$(5.1±0.7)×10^8$
S400A	√	+	93.1±2.3	98.3±1.8	ND	ND	+	$(2.2±0.0)×10^8$
Q401A	√	+	99.6±7.0	104.5±1.0	ND	ND	+	$(6.2±0.8)×10^8$
I403A	√	+	100.1±3.7	92.4±1.1	ND	ND	+	$(2.4±0.3)×10^8$
D404A	×	+	88.3±0.9	13.1±0.5	81.2±2.2	80.3±2.2	+	$(1.7±0.2)×10^8$
F405A	×	+	96.7±5.0	91.4±8.8	ND	ND	+	$(1.7±0.2)×10^8$
S406A	√	+	96.8±0.3	96.6±2.6	ND	ND	+	$(2.7±0.7)×10^8$
N407A	-	+	103.1±4.9	13.7±0.2	82.8±0.9	81.95±1.1	+	$(1.1±0.1)×10^8$
T379/F405A	×	+	99.4±3.3	96.8±1.0	ND	ND	+	$(2.4±0.3)×10^8$
N381/N385A	×	+	16.4±1.3	0	0	0	-	NA
N381/K389A	×	+	8.9±0.3	0	0	0	+	$(8.4±0.2)×10^6$
N381/Q401A	×	+	53.0±2.3	7.6±3.5	70.9±2.4	69.7±2.3	+	$(1.3±0.4)×10^8$
N381/I403A	×	+	51.8±0.4	11.0±0.3	65.7±1.3	64.2±1.1	+	$(1.4±0.2)×10^8$
N384/Y388A	×	+	7.0±1.3	0	0	0	-	NA
N385/K389A	×	+	152.8±0.7	94.1±0.6	ND	ND	+	$(3.9±1.0)×10^8$
N385/W393A	×	+	6.1±0.4	0	0	0	-	NA
K389/W393A	×	+	6.3±0.4	0	0	0	-	NA
D398/S400A	×	+	106.7±1.5	99.7±2.2	ND	ND	+	$(2.0±0.3)×10^8$
D398/Q401A	×	+	76.6±2.5	105.1±4.0	ND	ND	+	$(2.7±0.7)×10^8$
D404/S406A	×	+	82.5±1.9	11.2±2.4	83.8±1.3	82.6±1.1	+	$(3.5±0.4)×10^8$

[a] Residues contacts were analyzed in predicted postfusion structures of WT and the modified GP64s; [b]Virus infectivity was determined by a transfection-infection assay; ND, not done; NA, not available.